

The Interaction of Tetryl, a Nitroaromatic Explosive, with Bacterial Reaction Centres

Daniel Modafferi

A Thesis in the Department of Physics

Presented in Partial Fulfillment of the Requirements for the Degree of

Master of Science (Physics)

at

Concordia University

Montreal, Quebec, Canada

August 2018

© Daniel Modafferi



# Abstract

Tetryl, a nitroaromatic compound, was found to interact in two different measurable ways with bacterial reaction centre protein (BRC). The protein amplifies the reaction of tetryl occurring in the presence of detergent, producing a visible product with absorption peaks at 345 nm and 415 nm. BRC provides a location in the micelle with a rate 80-fold faster than in buffer with equal detergent concentration, and a location in the carotenoid binding site when carotenoid is absent with a rate 400-fold faster than in the bulk. The tetryl or its reaction product was also found to bind to the BRC near the bacteriochlorophyll dimer with micromolar level dissociation constant. The binding resulted in slowing down the charge recombination kinetics by modifying the light-induced structural changes. Up to 70% of the protein population can be made to recover with a rate constant of  $0.01\text{ s}^{-1}$ , about 100-fold slower than in the dark-adapted conformation.

Both these effects can be combined to design a bimodal biosensor. The change in absorbance at 350 nm can be used to detect tetryl in the ppb (parts-per-billion) concentration range, and photocurrents across a monolayer of BRC on an electrode could be affected by the presence of tetryl. Last, this interaction could be the starting point to the design of bio-hybrid charge-storage devices or completely artificial photosynthetic devices.

# Acknowledgements

I would first like to thank both my co-supervisors, Drs. Laszlo Kalman and Valter Zazubovits, for not only offering their scientific insight and experience to help me build and improve all aspects of my scientific career, but also for their advice and care for my future and my professional growth. I would also like to thank my committee members, Drs. Claudine Gauthier and Pablo Bianucci for their time, intellect and helpful feedback.

I am happy to have been helped in my research by a group of fellow students who also provided support and friendship. I would like to specifically underline both undergraduates, Kelly and Dereck's work on my specific project, and of course Ali, fellow master's student, for collaborating with me to keep the entire lab going, on all general lab procedures.

Last, writing a thesis also requires support from close ones. My family and close friends have kept me on track and motivated to achieve all my goals, including this one. I am extremely fortunate that my emotional support includes some great minds, and would like to specifically thank my mother, Manon, for developing my mathematical mind my entire life, and more recently for her extremely patient help on some of the mathematics in this work, and Ben, for his calming influence when I often needed it and for sharing his keen knowledge on writing and literature resource software methodology, saving me from hours of frustration and mild incompetence facing some ubiquitous computer software.

# Table of Contents

1 Introduction .....	1
1.1 Photosynthesis .....	1
1.1.1 Plant vs bacterial photosynthesis .....	1
1.2 Reaction centre .....	4
1.2.1 Electron transfer in BRC .....	5
1.2.2 Charge recombination .....	7
1.3 Nitroaromatic explosives .....	11
1.4 Bio-inspired nanodevices .....	13
1.4.1 Biosensors .....	13
1.4.2 Bio-hybrid or artificial solar cells.....	14
1.5 Objective .....	14
2 Experimental .....	16
2.1 <i>Rhodobacter sphaeroides</i> growth .....	16
2.2 Reaction centre purification .....	19
2.2.1 Cell membrane fragmentation.....	19
2.2.2 Solubilization of BRC .....	19
2.2.3 Isolation of crude BRC.....	19
2.2.4 Column purification .....	20
2.2.5 Concentration .....	20
2.3 Optical spectroscopy.....	21
2.3.1 Basic principles.....	21
2.3.2 Spectrophotometer .....	22
2.3.3 Absorption Spectrum of the BRC .....	23

2.3.4 Optical Spectroscopy Experiments .....	25
2.4 Data analysis .....	26
2.4.1 Kinetics .....	26
2.4.2 Spectral deconvolution .....	28
2.4.3 Ligand binding curves.....	28
3 Results.....	30
3.1 Tetryl product formation amplified by BRC.....	30
3.1.1 Monitoring the coloured tetryl product formation: Absorbance spectroscopy.....	31
3.1.2 Kinetics of product formation.....	36
3.2 Effect of tetryl on BRC charge recombination kinetics .....	41
4 Discussion.....	46
4.1 Reaction of tetryl with nucleophile-containing detergents.....	46
4.1.1 Probing the environment: Absorbance spectra of picric acid .....	47
4.1.2 Product identification: Absorbance spectra of reaction products.....	47
4.1.3 Reagent determination: reaction kinetics with LDAO .....	48
4.2 Evidence of tetryl binding to BRC – concentration dependence.....	49
4.3 Location of interactions .....	50
4.3.1 Tetryl-detergent reaction.....	50
4.3.2 Charge recombination .....	52
4.4 Proposed mechanism.....	54
4.5 Effect of interaction – biosensing signal amplification and charge-storage capacity.....	56
4.5.1 Biosensing .....	56
4.5.2 Charge storage device.....	58
5 Conclusion.....	59
6 References .....	60

# 1 Introduction

## 1.1 Photosynthesis

A vital process for sustaining all life on Earth, photosynthesis is a process in plants and bacteria where electromagnetic radiation in the form of light is converted to electrochemical energy. In bacteria and other primitive forms, only a proton gradient is formed across a membrane as a result. This proton motive force supplies the electrochemical potential necessary for powering the production of ATP, the molecule most consumed for anabolic cellular processes requiring energy.<sup>1</sup> In plants, this process produces ATP and NADPH as well, high energy molecules consumed for the fixation of CO<sub>2</sub> into glucose, a nutrient used by the plant itself and any other life forms consuming the plant. Plants also evolved from their more primitive relatives to oxidize water using a manganese ion cluster, producing oxygen as a by-product. This step in evolution shaped the atmosphere to allow it to sustain life as it is known today, and is supposed to have developed between 3.0 and 3.5 billions years ago.<sup>2</sup>

### 1.1.1 Plant vs bacterial photosynthesis

In plants, algae, and cyanobacteria, photosystem II (PSII) protein is responsible for the initiation of light-activated electron transport. It is found in the thylakoid membrane, in the chloroplast, the organelle specializing in photosynthesis. To capture the energy from light, the protein uses chlorophyll cofactors, highly conjugated ring structures called porphyrins with a central magnesium ion. The central chlorophyll pair, found in the photosystem II protein, can be excited by light directly, or by resonance energy transfer from the antenna complexes, shown in Figure 1, containing many chlorophyll molecules to optimally harness light energy. The electron transfer is non-cyclic, referred to as following a Z-scheme, as shown by Figure 2. As the electron is transferred through PSII from chlorophyll to plastoquinone, the mobile electron transporter, it is replenished by the oxidation of water into oxygen by a manganese containing complex. Plastoquinone transfers the electron to another protein complex in the membrane, cytochrome complex  $bf_6$ , where plastocyanin then carries the electron through the membrane to photosystem I (PSI), which will be used to reduce the chlorophyll in PSI that has been excited and oxidized by light. The electron from chlorophyll in PSI is transported by ferredoxin to the NADPH reductase enzyme, where it will be used to reduce NADP<sup>+</sup> to NADPH, an oxidizing agent necessary for the fixation of CO<sub>2</sub> into sugar molecules for energy storage. Throughout the chain, the favourable, free-energy releasing redox reactions are paired with energy-requiring proton transport processes across the membrane, generating a proton motive force. The plastoquinone cycle also helps generate the proton motive force. Plastoquinone receives two protons from the chloroplast stroma when being reduced at PSII and releases them into the thylakoid

lumen when transferring its two electrons to cytochrome  $bf_6$  complex. The potential energy created is used to synthesise ATP using ATP synthase, also present in the thylakoid membrane.<sup>3</sup>

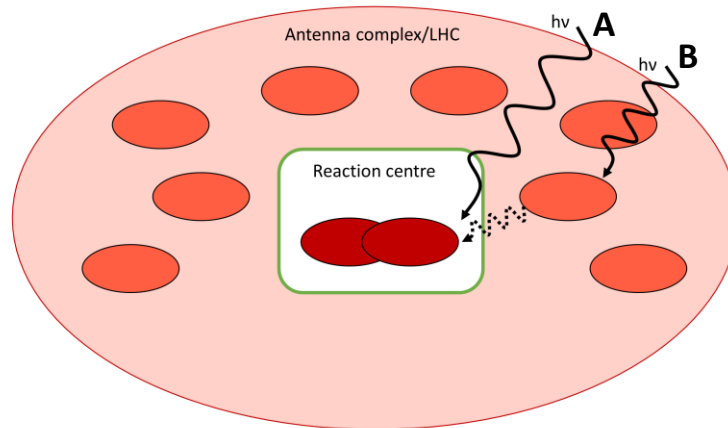


**Figure 1: Antenna complex, known as the light harvesting complex (LHC), surrounding reaction centre, found in both plants and purple bacteria. Light can be harvested by either the central chlorophyll or bacteriochlorophyll molecules (dark red) part of any reaction centre protein, either PSII, PSI or bacteriochlorophyll (A), or by the chlorophyll or bacteriochlorophyll molecules part of the LHC (light red), and then transferred through a resonance energy transfer process to the central pair (B).**

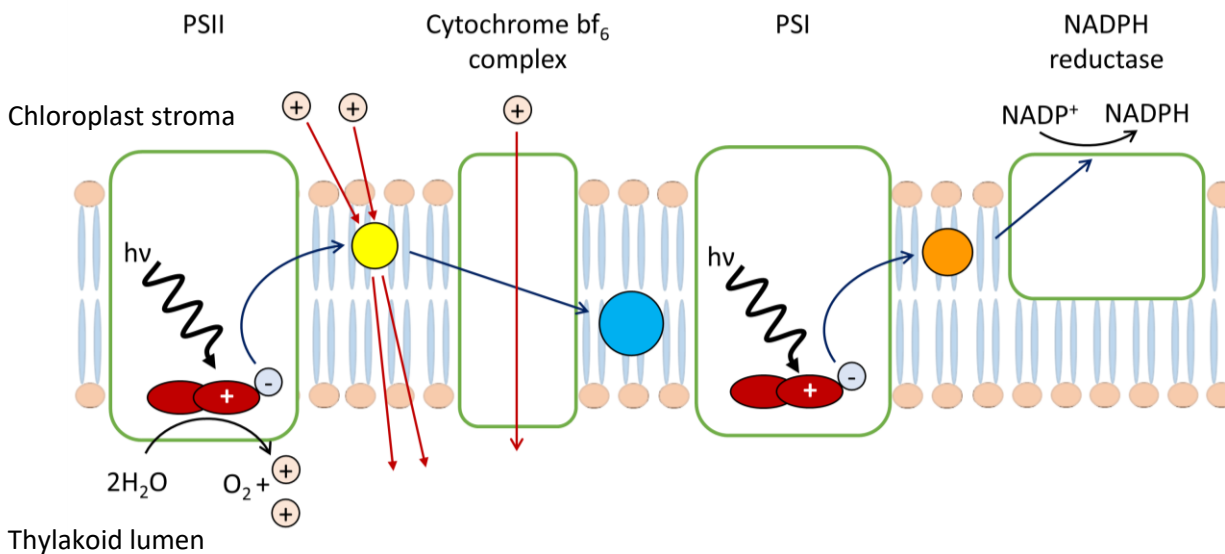


**Figure 2: Z-scheme of the electron transfer chain in photosynthesis of plants and algae. Blue arrows represent the electron pathway, red arrows represent proton transport across the membrane. Electron**

carriers shown: red: chlorophyll special pairs, yellow: plastoquinone, blue: plastocyanin, and orange: ferredoxin.

Anoxygenic photosynthetic organisms like purple bacteria contain bacterial reaction centres (BRC), pigment-protein complexes whose main features are analogous to those of the PSII from plants and algae. Since bacteria do not contain organelles, BRCs are found in the periplasmic membrane of the cell. Similar to PSII, BRC contains a bacteriochlorophyll pair that is excited by light or by resonance energy transfer from the antenna complex. However, there is no manganese complex to reduce the oxidized bacteriochlorophyll and oxidize water. Instead, the process is cyclic, seen in Figure 3. The electron from the bacteriochlorophyll dimer is transported by electron transfer cofactors to the ubiquinone, a mobile electron transporter analogous to plastoquinone in PSII. The double reduced double protonated ubiquinone (ubiquinol) travels through the membrane to the cytochrome  $bc_1$  complex. The ubiquinone transport is also responsible for shuttling protons from the cytosol to the extracellular space, using the same mechanism as for plastoquinone in plants. The cytochrome molecule is responsible for returning the electron back to the oxidized bacteriochlorophyll dimer, rather than reducing  $NADP^+$  as in plants. Thus, the electron transport chain in bacteria does not create reducing power as it does in plants, nor does it oxidize water into oxygen. It simply creates a proton gradient, by pairing the favourable redox reactions to unfavourable proton transport against its electrochemical potential. The potential energy generated by this gradient is used as energy for many anabolic processes.<sup>1</sup>

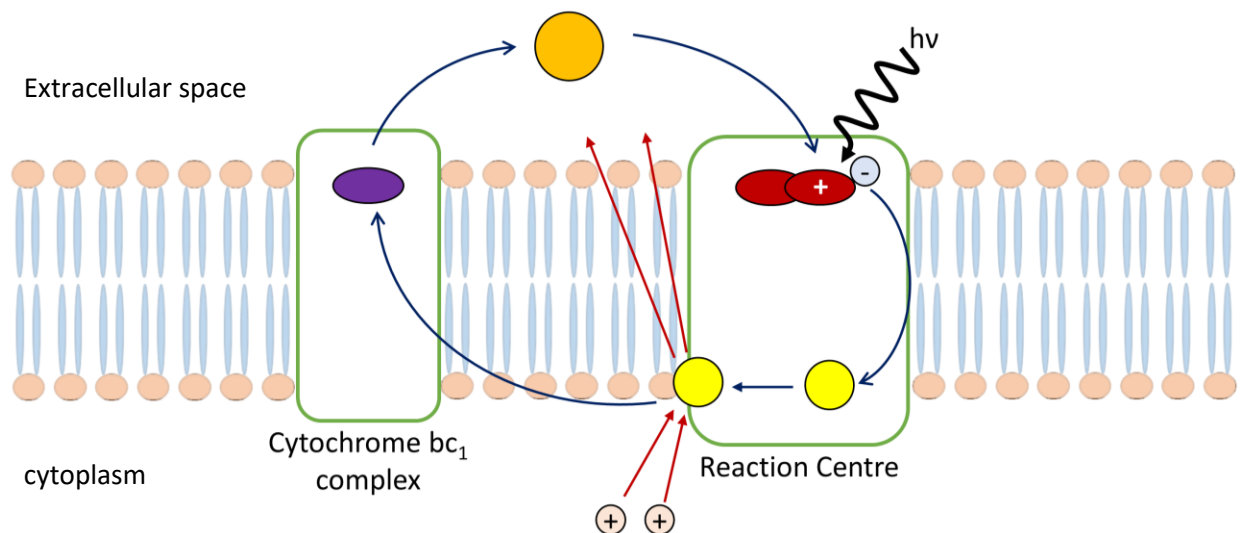


Figure 3: Scheme of cyclic electron transfer in purple bacteria photosynthesis. Blue arrows represent the electron pathway, red arrows represent proton transport across the membrane. Electron carriers

**shown: red: bacteriochlorophyll dimer, yellow: ubiquinone, purple: iron-sulfur clusters, and orange: cytochrome c.**

## 1.2 Reaction centre

As mentioned in the previous section, the initialization of the conversion of light into usable energy for biological purposes is made by proteins called reaction centres. The existence of these proteins, found relatively well conserved in all photosynthetic organisms, has been known since the 1930s. Emerson was able to quantify the reduction of carbon dioxide occurring when these chlorophyll-containing biomolecules were exposed to precise quanta of light.<sup>4</sup>

In nature, reaction centres are divided into two categories: type I and type II, based on their structure and terminal electron acceptors. All type II reaction centres operate similarly. A central chlorophyll molecule or pair is excited by a photon. The excited electron in the molecule becomes a stronger reductant, allowing it to be transferred to another acceptor molecule. Structurally, this acceptor molecule is a quinone, which receives two electrons and two protons to become fully reduced quinol.<sup>5</sup> To avoid the reverse transfer of an electron back to the primary chlorophyll, the protein scaffold is built optimally such that the redox potentials of the molecules would not allow the backwards electron transfer. Additionally, several other acceptors are present to form an electron-transfer chain, which separates the electron from its initial chlorophyll molecule. This redox chain provides the energy needed to generate the products of photosynthesis, whether it is the formation of a proton gradient or, for some type I reaction centres, the oxidation of a higher redox potential molecule such as NADPH. To regenerate the reduced chlorophyll, the protein could either receive an electron from an external protein complex source, or it could be transferred back in a cyclic mechanism.<sup>1,3</sup>

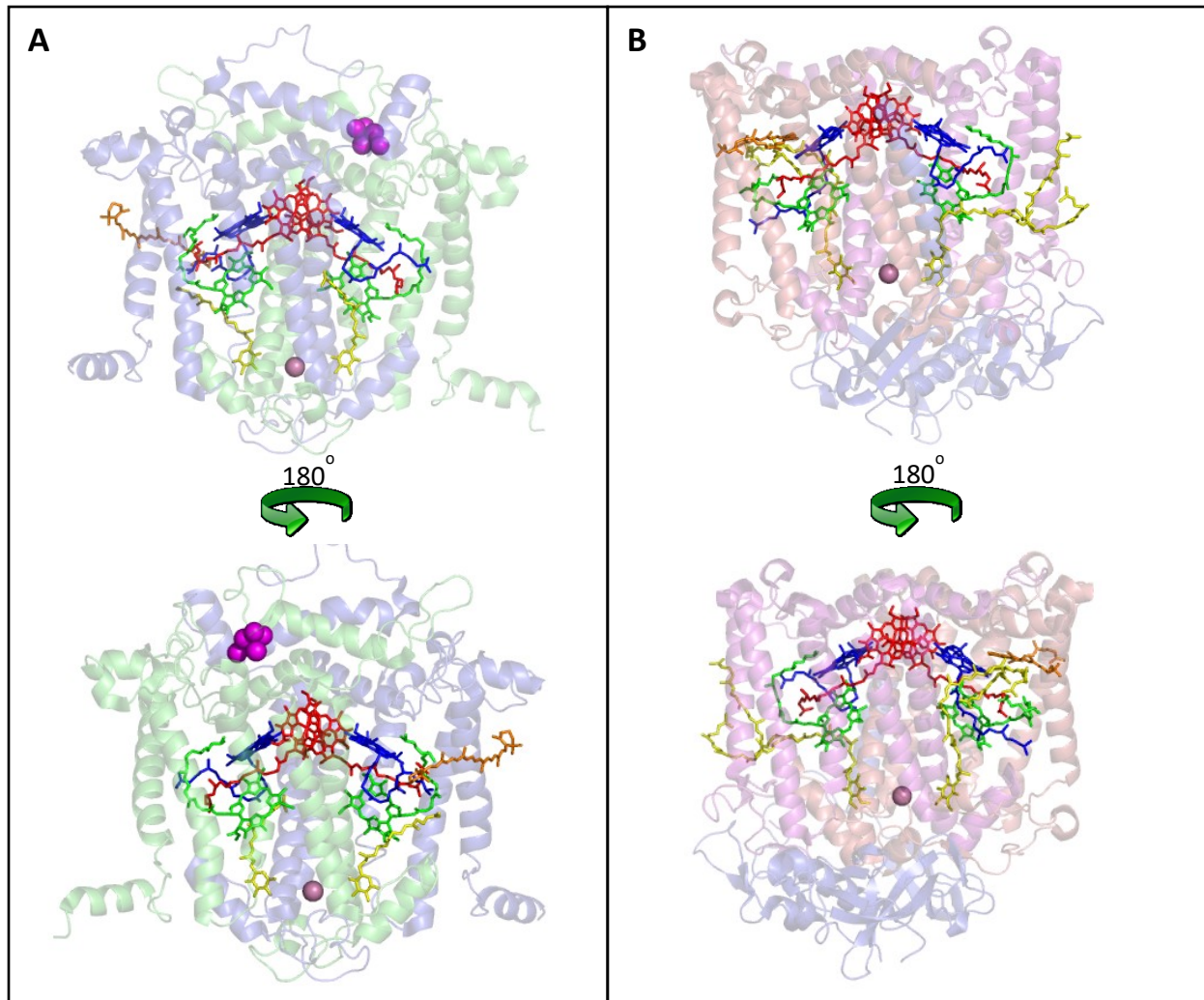


**Figure 4: Reaction centre cofactors involved in electron transfer. (A) Reaction centre of PSII from cyanobacteria, PDB access code 2AXT,<sup>6</sup> (B) BRC from purple bacteria *R. sphaeroides*, PDB access code 3I4D.<sup>7</sup> Cofactors present are: chlorophyll/bacteriochlorophyll dimer (P) in red, chlorophyll/bacteriochlorophyll monomers (B<sub>A</sub> and B<sub>B</sub>) in blue, pheophytin/bacteriopheophytin (ϕ) in green, quinones (Q) in yellow, carotenoids in orange, iron in pink, oxygen-evolving complex in magenta.**

### 1.2.1 Electron transfer in BRC

It is important for the excited chlorophyll to be able to transfer its electron as far away and as quickly as possible. If the electron stays too close to the dimer, it risks transferring back to the dimer, resulting in loss of efficiency. Also, if the excited electron is unable to get transferred quickly enough from the dimer, it risks relaxing back to ground state, emitting fluorescent light or non-radiative energy (heat), also resulting in loss of efficiency in the ability to generate potential energy for ATP production and basic functions.<sup>8</sup>

Many factors contribute to the high efficiency of each of the electron transfer steps. The cofactors involved are porphyrins, large conjugated rings that can delocalize a charge. Also, because they are similar in structure, they have small differences in their redox potentials, making the Gibbs free energy of the transfer small. The small distance between cofactors minimizes the time of each transfer. By surrounding the cofactors in the hydrophobic core of the protein, the electron being transferred is in a lower dielectric environment than in an aqueous environment, also allowing for a more efficient transfer. All these factors allow for electron transfers that can approach the rate of a free-energy optimized electron, according to Marcus theory of electron transfer.<sup>9</sup>

#### *P to $\Phi$ electron transfer*

The 3 ps electron transfer from the bacteriochlorophyll dimer (P) to the bacteriopheophytin ( $\Phi$ ) is close to the maximum speed of a free-energy optimized electron transfer. As seen in Figure 5, the distance of 16.1 Å between the dimer and the pheophytin is too far to normally allow for such a fast transfer. It is believed that bacteriochlorophyll monomer A ( $B_A$ ) acts as an intermediate acceptor. Because the  $P^+B_A^-$  state cannot be observed in femtosecond spectroscopy, it is thought that the transfer rate from B to  $\Phi$  is much faster than the rate from P to  $B_A$ . This would prevent any reduced  $B_A$  from accumulating over time.<sup>8</sup>

#### *$\Phi$ to $Q_A$ electron transfer*

Because this step is over a larger distance than the monomer-mediated transfer from the dimer to the bacteriopheophytin, and the ubiquinone A molecule ( $Q_A$ ) contains a smaller ring than the porphyrin ring, the transfer occurs over a longer time. To account for the speed of 200 ps of electron transfer, which is still faster than the predicted rate using Marcus theory, it has been proposed that the nearby aromatic ring of the M252 tryptophan acts as a bridging mediator in the electron transfer (Figure 5).<sup>8</sup>

#### *$Q_A$ to $Q_B$ electron transfer*

The last electron transfer step in the charge separation process in RC is the transfer from  $Q_A$  to  $Q_B$  (Figure 5). To have a spontaneous electron transfer, there must be a difference in redox potentials between the donor and acceptor molecules. Since in this case, both molecules are identical, the difference in redox potential is due to the differences in environment surrounding both molecules.  $Q_B$  is in a more polar environment, and the iron ion is slightly closer to it, which stabilizes the negatively charged semi-reduced form of ubiquinone.<sup>8</sup>

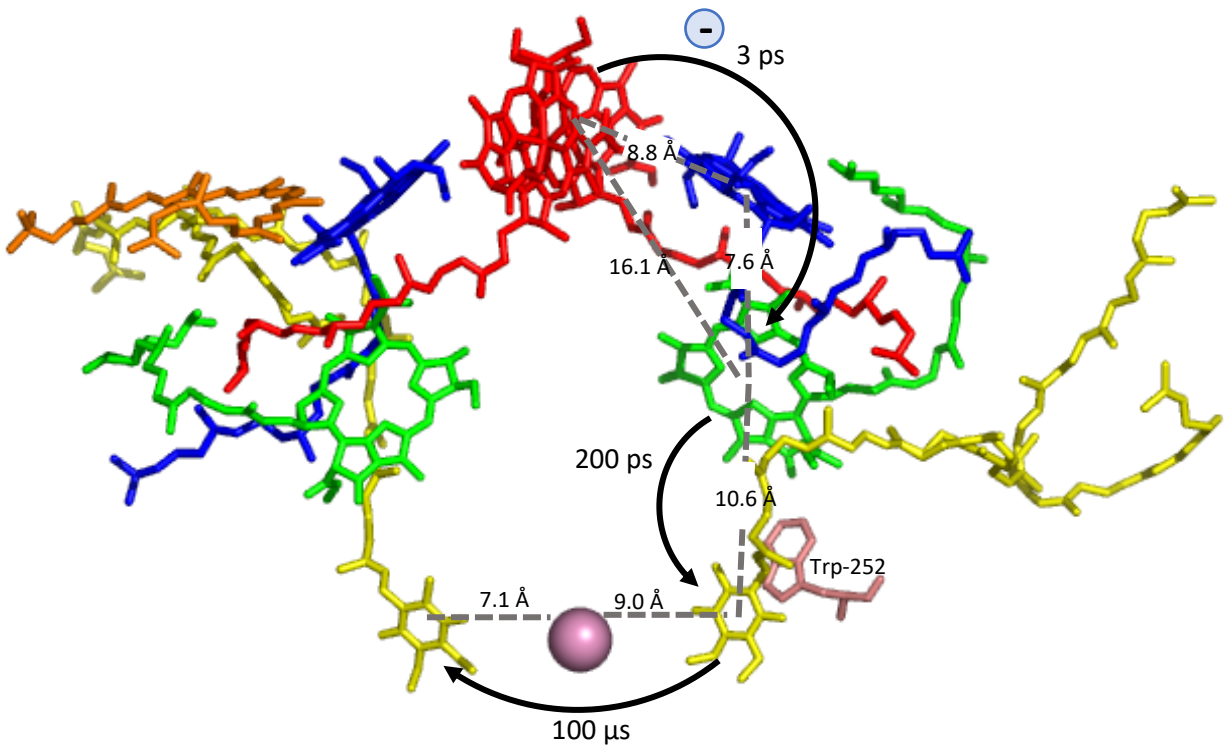


**Figure 5: Charge separation of BRC occurs by electron transfer between cofactors of the A branch. Bacteriochlorophyll dimer in red, bacteriochlorophyll monomers in blue, bacteriopheophytin in green, ubiquinone in yellow, carotenoid in orange, iron in pink sphere, Trp-252 is shown in salmon. PDB access code 3I4D.<sup>7</sup>**

### 1.2.2 Charge recombination

In vitro, in the absence of a pool of ubiquinone  $Q_B$  and a secondary electron donor, normally cytochrome, the charges generated on the dimer and quinone will recombine through the protein in the dark (Figure 6). The key to using these proteins as nanoreactors is to lengthen the time for this generated charge pair to recover. Naturally, the charge recombination process happens several orders of magnitude slower than the charge separation. The charge separation needs to be paired to a process with faster kinetics, or energy will be inefficiently lost to the charge recombination process. Thus, the slower the charge recombination, the more efficiently the photosynthetic cell draws usable potential energy from the charge separation.<sup>8</sup>

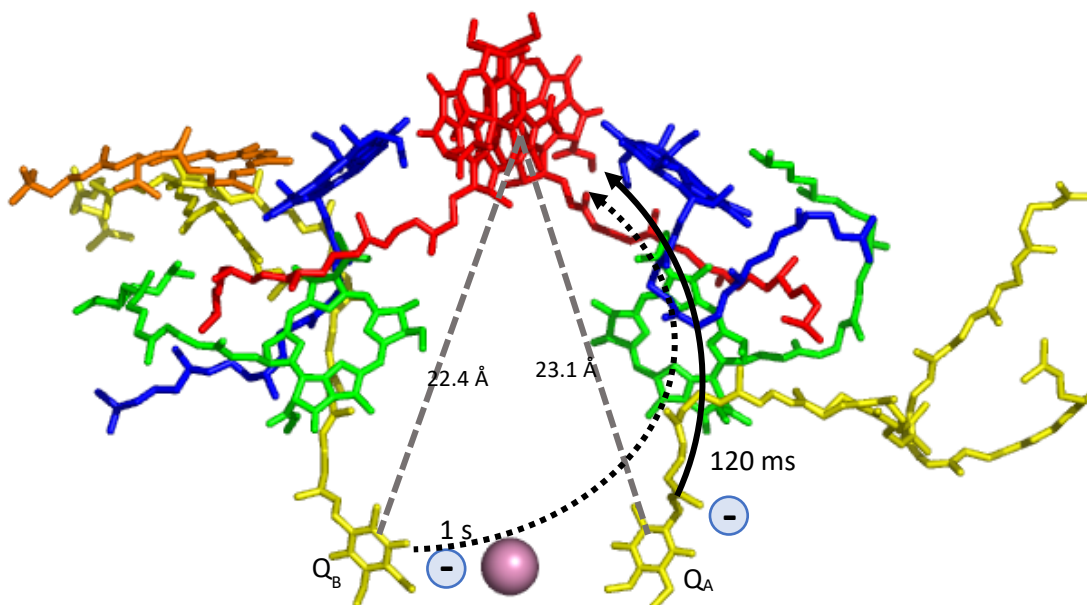


**Figure 6: Q<sub>A</sub> (full line) and Q<sub>B</sub> (dotted line) to P charge recombination. PDB access code 3I4D.<sup>7</sup>**

#### *Q<sub>B</sub> to P electron transfer*

Ubiquinone is less tightly associated to the BRC at the B site than at the A site. When Q<sub>B</sub> is present and the electron transfer from Q<sub>A</sub> to Q<sub>B</sub> is not inhibited, the charge recombines from Q<sub>B</sub> in 90% of the proteins, with a rate constant around  $1 \text{ s}^{-1}$ . It has been demonstrated that the recombination occurs predominantly through the indirect pathway, the electron traveling first back to Q<sub>A</sub> before re-reducing the dimer.<sup>10</sup>

The presence of polar residues near Q<sub>B</sub> is believed to stabilize the negatively charged Q<sub>B</sub>, lowering the recombination rate.<sup>8</sup> The long distance the electron needs to travel from Q<sub>B</sub> back to P is also responsible for the slow rate of this transfer.

#### *Q<sub>A</sub> to P electron transfer*

For the charge recombination from Q<sub>A</sub> to P to be observed, which is around an order of magnitude faster than the recombination from Q<sub>B</sub> to P, an electron transfer inhibitor is needed to replace the Q<sub>B</sub>, or the secondary Q<sub>B</sub> quinone, which is more loosely bound, must simply be removed. Many herbicides act as Q<sub>B</sub> displacers and cause the observable charge recombination to occur on a faster timescale.<sup>10</sup>

This charge recombination happens more quickly, with a rate constant of around  $10 \text{ s}^{-1}$ . Because of the larger difference in free energy between the P<sup>+</sup>IQ<sup>-</sup> and P<sup>+</sup>I<sup>-</sup>Q states, where I is an intermediate electron acceptor, the electron will with very high probability travel directly back to the dimer without the use of an intermediate electron acceptor.<sup>11</sup>

### *Conformational changes leading to slower charge recombination kinetics*

X-ray diffraction off crystals at cryogenic temperatures have shown that upon illumination, the protein undergoes a conformation change around the  $Q_B$ . A 150 ms pulse of light was sufficient to rotate the  $Q_B$  180° around the isoprene and shift it by 5 Å from its position in dark-adapted protein (Figure 7). This change brings the  $Q_B$  ring closer to the positively charged iron ion, and also adds hydrogen bonds to the L223 Ser and L190 His. Because of the stabilization of the negative charge on  $Q_B$  from the closer proximity of the iron ion and the additional hydrogen bonds, the rate of recombination of the electron from the conformationally-changed  $Q_B$  is an order of magnitude slower than in the dark-adapted state, in the range of  $10^{-1} \text{ s}^{-1}$ . No changes in the amino acid chain were reported in this experiment, since illumination was performed on rigid crystals.<sup>12</sup>

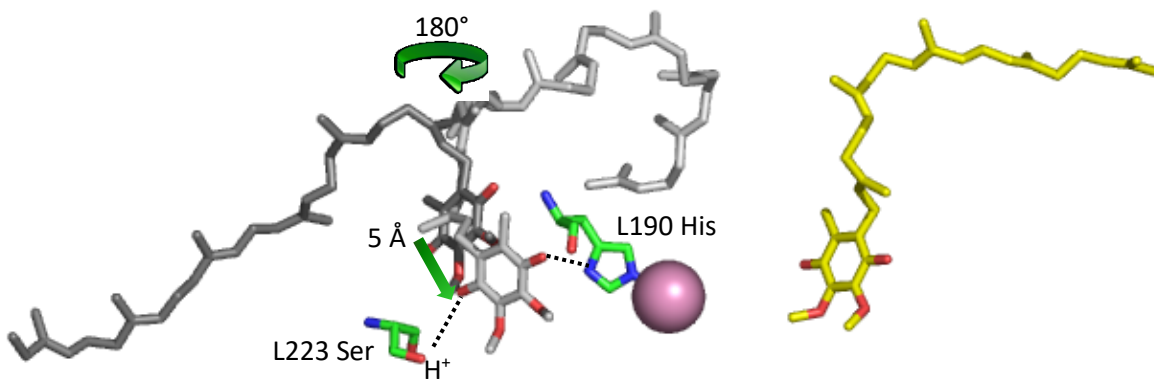


**Figure 7: Conformation changes around ubiquinone B from dark (black) to light-adapted (white) state. Rotation of 180° around isoprene and shift of around 5 Å occurs. Iron shown as pink sphere, and ubiquinone A in yellow. PDB structures 1AIJ for dark-adapted and 1AIG for light-adapted state.<sup>12</sup>**

More recently, it was found that conformational changes around the dimer have a more significant impact on the stabilization of the charge separated protein. The addition of hydrogen bonds around the dimer can disrupt favourable interactions that lower the energy of the charge on the dipole, which have been shown to slow the electron transfer from Q to P down to a rate an order of magnitude slower than for the conformational change around the quinone, in the range of  $10^{-2} \text{ s}^{-1}$ . Specifically, the rotation of the 2-acetyl group of the active bacteriochlorophyll dimer and the deprotonation of M210 Tyr stabilize the dimer.<sup>13,14</sup>

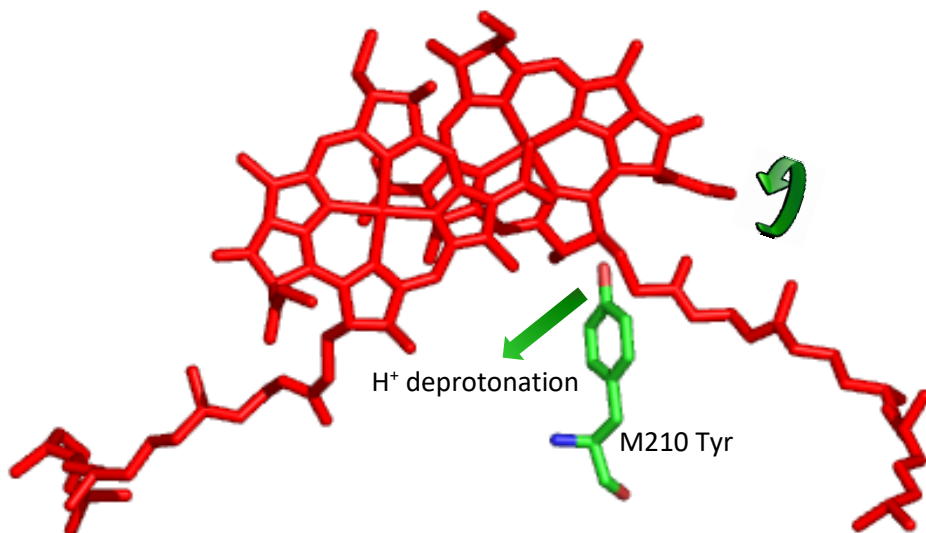


**Figure 8: Conformation changes around bacteriochlorophyll dimer occurring in light. Rotation of 2-acetyl group of dimer and deprotonation of M210 Tyr.**

The conformation changes occurring in the light occur consecutively. The changes around  $Q_B$  occur more rapidly. The conformation change is seen after only 150 ms illumination of BRC crystals.<sup>12</sup> Several orders of magnitude slower, with illumination in the minute time-scale, the conformational changes around the dimer are observable.<sup>13-15</sup> The mechanism of all light-induced conformational changes is represented in Figure 9.

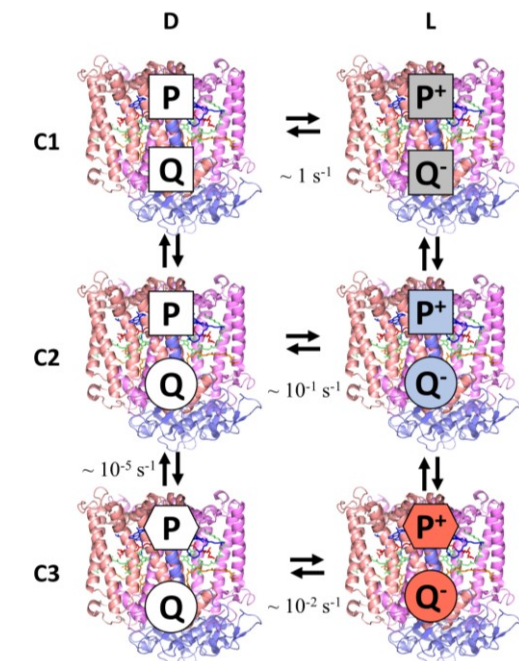


**Figure 9: Scheme of light-induced conformation changes of BRC. Protein on the left are in the dark, and on the right are  $P^+Q^-$  charge-separated protein in the light. C1, C2 and C3 conformers represent respectively the dark-adapted conformation, the light-induced conformation changes near the quinone, and light induced conformation changes near the dimer.**

### 1.3 Nitroaromatic explosives

Explosives are especially damaging weapons in that they are indiscriminate to victims. Civilian lives can be as targeted as military lives. Not only are they dangerous weapons in battlefields or in highly populated areas, but these chemicals penetrate skin and contaminate waters to act as toxins and mutagens, harming all living organisms.<sup>16</sup>

Nitroaromatic compounds are a class of explosives consisting of an aromatic ring with one or more nitro groups ( $\text{NO}_2$ ) as substituents. As compounds for organic synthesis, these chemicals have many uses. They are used as starting points for many different compounds, from herbicides to pharmaceuticals, to rubber and other materials.<sup>17</sup> The oxygen atoms in the nitro group share a negative charge through resonance, and the nitrogen atom is left with a positive charge, making it very electronegative. This has the effect of delocalizing electrons from the aromatic ring and favours the substitution of groups at the meta position of the aromatic ring.

The nitro groups are very sensitive to a homolytic radicalization reaction that removes them from the ring. This reaction is followed by a series of very exothermic redox reactions, resulting in the rapid degradation

of the entire molecule into nitrogen gas, carbon dioxide and water.<sup>18</sup> Because the reaction creates numerous products, contributing to a large increase in entropy, and these products are very stable, contributing to a large increase in enthalpy, there is an extreme release of energy, seen as a damaging explosive blast.

As seen in Figure 10, nitroaromatic compounds are similar in structure to a class of herbicides acting as quinone inhibitors called phenolic herbicides. Competitive binding to proteins works by having similar structures bind to a binding site instead of the native molecule. DNOC and other similar molecules bind to the secondary quinone site,  $Q_b$ , where they prevent binding of quinone, speeding up the charge recombination. In living photosynthetic organisms, this prevents the electron from reaching the secondary quinone, which will interrupt the electron transfer chain and prevent a proton motive force from accumulating.<sup>19</sup>

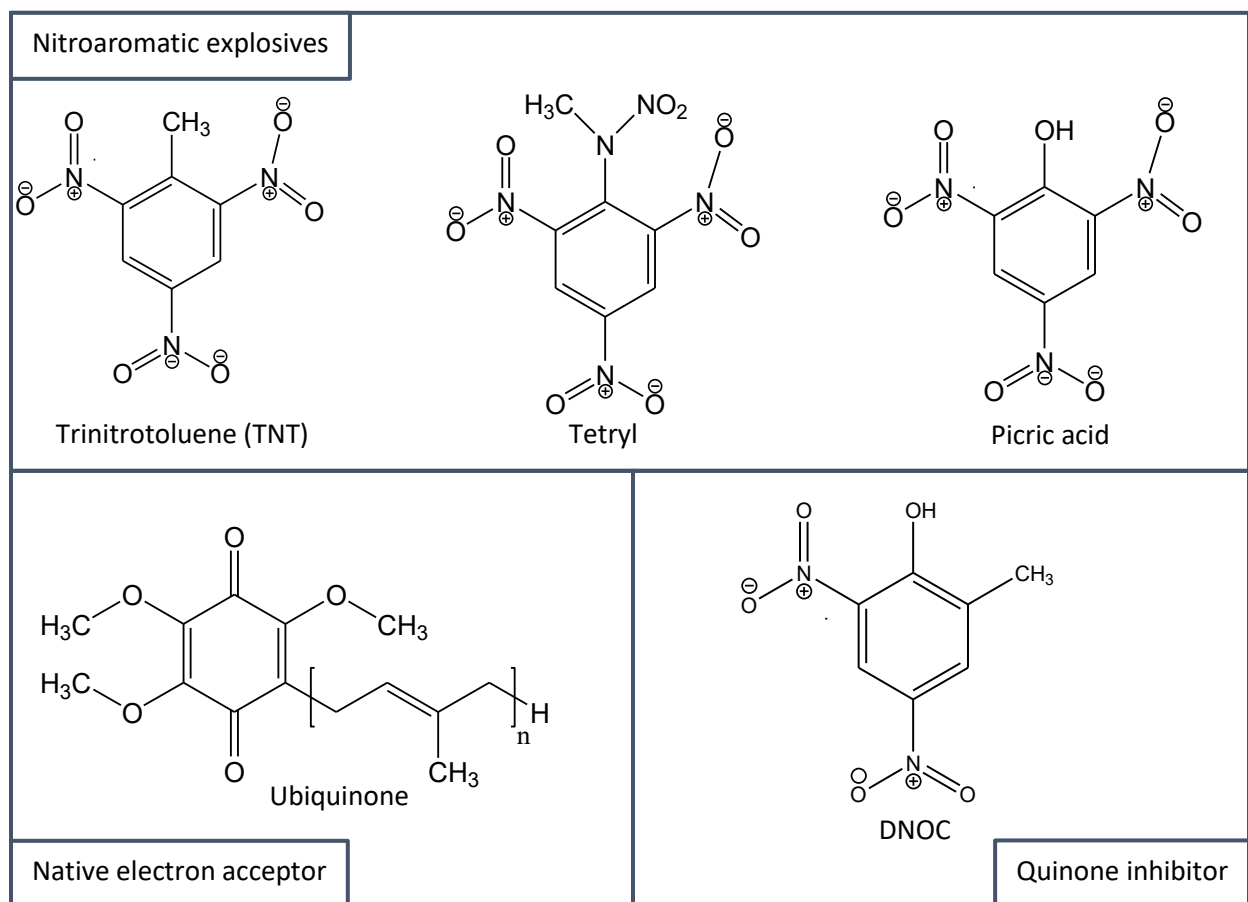


**Figure 10: Chemical structures of some nitroaromatic explosives, ubiquinone and DNOC, a quinone inhibitor.**

## 1.4 Bio-inspired nanodevices

Over millions of years of evolution, organisms have evolved near-perfected nanomachinery capable of higher efficiency at precise functions than what scientists can engineer themselves in a laboratory. By understanding the mechanism of these machineries in their native organisms, scientists hope to extract the essential parts required and improve them for purposes envisioned for human use: drug delivery, diagnostics, biosensing, energy production are a few other uses.

### 1.4.1 Biosensors

Generally, biosensors utilise protein or DNA to bind to a target molecule. The interaction between the sensor and target must create a measurable signal, for example using spectroscopy or electrochemistry, to name a few possible detection modalities. An important component of the biosensor is that it is often on a surface or contains a synthetic component that will make the biomolecule sturdier and increase its shelf life, and even perhaps help amplify the signal.<sup>20</sup>

Immunosensors are very common biosensors, as they can be designed for any antigen, a fragment of a molecule to which an antibody binds. The antibodies are usually covalently linked to a molecule that can adhere to an electrode. Luminescence techniques such as fluorescence are often used for the detection signal. Either by covalently linking a fluorophore or enzyme that can make a luminescent product, or by competitive inhibition with a fluorescent or luminescent analog, the presence of explosive bound to the antibody will produce an optically measurable signal. The inevitable problems that arise from antibody-based biosensors are that they are very labour-intensive and rely heavily on the use of animal models, which raises ethical questions, costs and production time.<sup>16</sup>

Previously, biosensors based on PSII have been made to detect herbicides. Thylakoid membranes were used in an electrochemical cell, and the ability of the layer of reaction centres to transfer an electron in the light was measured as the signal. In the presence of a herbicide, the electron transfer was blocked, which would decrease the measured photocurrent.<sup>21</sup>

Additionally, PSII was used to detect TNT and picric acid. A gold surface was functionalized with TNT, by adding a sulfur-based compound linked to NHS. The sulfur would bind very strongly to the gold surface, whereas the NHS would form a covalent bond with a lysine residue on the protein. Like herbicides, these explosives were found to reduce the photocurrent of the device constructed with PSII.<sup>22,23</sup>

#### 1.4.2 Bio-hybrid or artificial solar cells

The highly efficient light-capturing machinery of photosynthetic reaction centres is also studied to understand how to use sunlight for energy production. The sun is a virtually inexhaustible source of energy. Plants utilise this to store energy as electrochemical potential gradients or by re-reducing strong reducing agents. This energy conversion requires water as fuel, and as waste produces oxygen. It is unsurprising many researchers seek to find ways to adapt this clean and renewable process to human energy requirements.

Artificial photosynthesis uses the principles studied in natural photosynthesis to produce completely synthetic molecular machines that have the essential parts of reaction centres and can undergo light-induced electron transfer. The design of these devices often begins with a porphyrin ring, due to its high extinction coefficient and capacity for light-induced electron transfer. The electron donor porphyrin or another system with similar properties is usually paired to an electron acceptor molecule with an appropriate redox potential for electron transfer to occur, such as fullerene or pyrene. Not only are the electron carriers important, but their location and relative position to each other, as well as the environment they are in have a huge influence on the efficiency of the device. These devices are assembled into larger molecules or supramolecular structures by covalent linking or self-assembly.<sup>24</sup> There is a constant need to improve robustness, efficiency of the electron transfer, and simplicity of the design for higher yields and cheaper fabrication processes.

Bio-hybrid designs will use these photosynthetic proteins as a starting material, and modify them through covalent cross-linking, mutagenesis or change their environment to optimize the charge separation process or lengthen the charge recomb. In a previous study done by our group, the changes in the environment of the cofactors in the protein, made either by changing lipid composition through using different lipids in micelles or by liposomal encapsulation, or by site-directed mutagenesis, were found to impact the  $P^+Q^-$  charge recombination. By stabilizing the charge separated state of the reaction centre, one can improve the capacity for the protein to act as a molecular solar-charged battery or capacitor, where a charge is separated across a membrane, and its recombination drives other energy-costly processes.<sup>13–15</sup>

#### 1.5 Objective

Q-site inhibiting herbicides, such as DNOC, are similar in structure to nitroaromatic explosives. By analogy, these explosives could also have inhibitive properties on the reaction centre, by binding to the quinone

site. It has already been demonstrated that TNT and picric acid can be detected by a PSII-based biosensor<sup>22,23</sup>

Because of its evolutionary ties to PSII, the BRC could be used as an alternative to PSII-based systems. *Rhodobacter sphaeroides* bacteria are relatively easy to grow anaerobically in large abundance, and their reaction centres are more robust than PSII in plants.<sup>25</sup> If any nitroaromatic explosive interacts with the protein, in proximity to the electron-carrying cofactors, it can likely be detected through a change in the photocurrent observed in a device constructed from this protein. Any changes in the environment of the absorbing cofactors or of the absorbing aromatic rings of the explosives caused by the interaction could also be detected in the absorbance spectrum of either the protein or the explosive (see section 2.3

Additionally, knowing the precise interaction location and biophysical mechanisms involved could help gain knowledge on the functioning of the electron transfer and recombination in bacterial reaction centres. This could be an important point in the design of a bio-mimetic or bio-hybrid device used for the storage of solar energy.

My project focused on the interaction of tetryl, a nitroaromatic explosive, and bacterial reaction centre for two purposes. First, any observable effect of the interaction could be used in the conception of a biosensor for tetryl. The formation of a product detectable by simple absorbance spectroscopy could be one mode of detection. If the explosive influences the charge recombination, the change in photocurrent caused by the presence of the explosive could be a second mode of detection. Second, if the tetryl stabilizes the charge separation, the interaction could be used in the creation of a simple solar-powered charge storage device.

## 2 Experimental

### 2.1 *Rhodobacter sphaeroides* growth

Growth medium was prepared according to recipe (Table 1). Medium was poured into 1 L glass bottles and autoclaved for 30 minutes, at 120°C in a Steris Amsco Century SV-120 Scientific Prevacuum Sterilizer autoclave. Medium was cooled before cells were added aseptically over a flame. Bottles were filled to the top so that as little oxygen as possible remains in the bottle.

Cells were incubated in the dark for 4 to 6 hours, for all the oxygen dissolved in the medium to be consumed. Then, cells were grown anaerobically at 30°C under light produced by incandescent bulbs, for 2 to 3 days. Cells were then pelleted using a Beckman J2-HS centrifuge, by spinning at 6,000 x g for 25 minutes using a Beckman JA-10 rotor. Pellets were kept frozen at -20°C until the purification process.

**Table 1: Recipes for solutions and media for bacterial anaerobic photosynthetic growth.**

<b>Solution</b>	<b>Product</b>	<b>Amount</b>	<b>Instructions</b>
<b>Growth medium (4 L)</b>	casamino acids	4 g	Dissolve all in distilled water Dilute to 4 L
	growth factor	4 mL	
	concentrated base	80 mL	
	potassium succinate	40 mL	
	phosphate buffer	80 mL	
	ammonium sulphate	25 mL	
<b>Growth factor (100 mL)</b>	biotin	2 g	Dissolve biotin and bicarbonate in 100 mL distilled water Add nicotinic acid, thiamine-HCl and PABA one at a time Boil to dissolve Autoclave
	sodium bicarbonate	50 mg	
	nicotinic acid	100 mg	
	thiamine-HCl	50 mg	
	para amino benzoic acid (PABA)	100 mg	
<b>Concentrated base (2 L)</b>	potassium hydroxide	12 g	Stir potassium hydroxide and NTA in 1 L distilled water for 20 minutes Let sediment, decant and discard pellet Add magnesium sulphate, wait until dissolved Add calcium chloride, wait until dissolved Add ammonium molybdenate 1 mL at a time, wait until dissolved Add ferrous sulphate, wait until dissolved Add metals 44 Dilute to 2 L with distilled water Adjust pH to 6.7 using 5% KOH
	nitrilotriacetic acid (NTA)	20 g	
	magnesium sulphate-heptahydrate	58 g	
	calcium chloride-dehydrate	6.8 g	
	ammonium molybdenate solution	4 mL	
	ferrous sulphate-heptahydrate	200 mg	
	metals 44	100 mL	
<b>Ammonium molybdenate (40 mL)</b>	ammonium molybdenate	184 mg	Dissolve in 40 mL distilled water

Solution	Product	Amount	Instructions
<b>Metals 44 (100 mL)</b>	EDTA	200 mg	Dissolve all in distilled water Adjust to 100 mL
	zinc sulphate- heptahydrate	1.1 g	
	ferrous sulphate- heptahydrate	500 mg	
	manganous sulphate- monohydrate	150 mg	
	cupric sulphate- pentahydrate	40 mg	
	cobalt chloride- hexahydrate	37 mg	
	boric acid	12 mg	
	sulphuric acid, 6N	150 µL	
<b>Potassium succinate (1 L)</b>	succinic acid	200 g	Stir succinic acid in distilled water In separate beaker, dissolve potassium hydroxide in distilled water Place succinic acid in ice bath Add potassium hydroxide in small increments Adjust pH to 6.8-7.0 Dilute to 1 L
	potassium hydroxide	200 g	
<b>Phosphate buffer (1 L)</b>	K <sub>2</sub> HPO <sub>4</sub>	115 g	Dissolve in distilled water Dilute to 1 L Adjust to pH 6.8 using NaOH
	KH <sub>2</sub> PO <sub>4</sub>	45 g	
<b>Ammonium sulphate (500 mL)</b>	ammonium sulphate	50 g	Dissolve in distilled water Adjust pH to 7.0 with ammonium hydroxide Dilute to 500 mL

## 2.2 Reaction centre purification

Membrane-bound bacterial reaction centre proteins are found naturally in *R. sphaeroides*. The protein was extracted from the frozen pellets of cells collected as described in the previous section (2.1

### 2.2.1 Cell membrane fragmentation

Approximately 75 g of frozen pelleted cells were resuspended in 200 mL 10 mM Tris buffer, pH 8.0. Once thawed and properly resuspended, the cells were placed in an ice bath and sonicated using a Heat Systems Inc. XL-2020 Ultrasonicator at 240 Watts, in bursts of 10 seconds with 10 seconds rest, for 1 hour. The lysed cells solution was adjusted to 0.1 M NaCl, 1 mM EDTA and 0.25% N,N-dimethyldodecylamine N-oxide, or LDAO (no LDAO was added when R26 cells were used). The cell lysate was centrifuged in 25 mL screw-cap bottles for 2h45 minutes, at 45,000 rpm, using a Beckman-Coulter Optima XL-100K Ultracentrifuge, with a Ti-70 rotor. The pelleted fragmented cell membrane was collected.

### 2.2.2 Solubilization of BRC

The cell fragments were resuspended in TEN buffer (15mM Tris, pH 8.0, 1 mM EDTA, 0.1 M NaCl), in a volume equal to the volume of supernatant collected from the previous centrifugation step. To solubilize the membrane-bound BRC protein, the solution was brought to 0.65% LDAO concentration, and stirred for 10 minutes at 26°C. The solution was centrifuged again with a Beckman-Coulter Optima XL-100K Ultracentrifuge and a Ti-70 rotor, at 45,000 rpm for 2 hours 15 minutes. The supernatant containing the solubilized BRC was kept.

### 2.2.3 Isolation of crude BRC

To the solubilized BRC solution, LDAO was added to obtain 1% concentration. Solution was brought to 30% ammonium sulphate and stirred for 10 minutes at room temperature to precipitate the BRC protein. Solution was centrifuged in a Beckman J2-HS centrifuge with a JA-17 rotor for 10 minutes at 10,000 rpm. BRC in floating pellet were collected.

Pellets were resuspended in TEN. To approximate the concentration of bacteriochlorophyll in the resuspension, the optical density-volume (ODV) was used. The ODV is the measure of the absorbance or optical density multiplied by the volume of sample. The volume of TEN added was measured to obtain an ODV<sub>800</sub> of 5. Resuspension was stirred for 2 hours. Solution was dialysed in 4 L TL<sup>0.1</sup>E buffer (15 mM Tris, pH 8.0, 0.1% LDAO, 1 mM EDTA) overnight at 4°C.

#### 2.2.4 Column purification

The next day, crude BRC solution was further purified using Toyopearl DEAE-650M resin packed in a column. The DEAE beads were first washed 3 times with approximately 500 mL TL<sup>0.1</sup>E, then packed in a column. The BRC was diluted 2 to 3-fold and was loaded onto the column using a Welch Riestchle Thomas Model 3100 peristaltic pump. The BRC was washed with TL<sup>0.1</sup>E for 30 minutes. Flowthrough was collected in a Spectra/Chrom CF-1 fraction collector, and spectrum was recorded with a Varian Cary 5000 spectrophotometer, from 250 nm to 1000 nm. After the wash, the BRC was eluted with a NaCl gradient, from 0 mM to 250 mM NaCl in TL<sup>0.1</sup>E. Eluent fractions containing A<sub>800</sub>/A<sub>280</sub> ratio of at most 2.0 were pooled and collected. Pooled BRC sample was dialysed overnight in 4 L TL<sup>0.025</sup>E (15 mM Tris, 0.025% LDAO, 1 mM EDTA), at 4°C.

#### 2.2.5 Concentration

Dialysed sample was concentrated using Amicon Stirred Ultrafiltration Cell Model 8050. A cellulose filter paper was placed in the filtration apparatus and soaked with distilled H<sub>2</sub>O. The purified BRC sample was added to the filtration apparatus, and 20 psi (138 KPa) of compressed air was used to push the BRC through the filtration system. The sample was concentrated to a final concentration around 100 µM, as determined by the absorbance spectrum of the sample. The concentrated BRC was separated into aliquots of 500 µL in black microcentrifuge tubes. Tubes were labeled with the concentration, A<sub>800</sub>/A<sub>280</sub> ratio, and date, and stored in a -20°C freezer until further use.

**Table 2: Recipes for solutions and buffers for BRC purification.**

<b>solution</b>	<b>product</b>	<b>amount</b>	<b>instructions</b>
<b>TEN (4L)</b>	Tris-HCl, 1 M, pH 8.0	40 mL	Mix all Dilute to 4 L
	ethylenediaminetetraacetic acid (EDTA) in Tris-HCl, pH 8.0	40 mL	
	sodium chloride	23.2 g	
<b>TLE (4 L)</b>	Tris-HCl, 1 M, pH 8.0	40 mL	Mix all Dilute to 4 L
	LDAO	13.3 mL (for 0.1%) 3.3 mL (for 0.025%)	
	ethylenediaminetetraacetic acid (EDTA) in Tris-HCl, pH 8.0	40 mL	
<b>Tris-HCl, 1 M, pH 8.0 (1 L)</b>	Tris	121.14 g	Dissolve in distilled water Adjust to pH 8.0 with concentrated HCl Dilute to 1 L
<b>EDTA in Tris-HCl, pH 8.0 (1 L)</b>	Tris Na <sub>4</sub> EDTA-dihydrate	60.57 g 41.621 g	Dissolve tris in distilled water Adjust to pH 8.0 with concentrated HCl Dissolve EDTA in tris solution Adjust to pH 8.0 with Concentrated HCl Dilute to 1 L

## 2.3 Optical spectroscopy

In optical spectroscopy, the interaction between light and matter is used to study molecules. Each molecule will have a unique spectral signature that is sensitive to the environment. This tool can be used for the identification of molecules and can give insight on the nature of its environment.

### 2.3.1 Basic principles

In quantum mechanics, light can be described as both a wave and a discrete amount of matter, called photons. The energy of a photon is related to its wavelength ( $\lambda$ ):

$$E = hc/\lambda$$

Light can interact with matter it hits. Electrons in atoms and molecules are in orbitals of discrete energy levels. If the electron receives energy equal to the energetic difference between the orbital it is currently on and a higher energy orbital, the electron can absorb that energy and get excited to a higher orbital. A photon with a specific wavelength matching the energy of the orbital transition of the electron will be absorbed by the molecule.<sup>26</sup>

The number of photons a sample will absorb will depend on the quantity of molecules in the light's pathway. It will be proportional to the concentration of the molecule ( $c$ ) and the pathlength it travels through the sample ( $l$ ). Additionally, there is a probability that the absorbance will occur, called the molar absorptivity, or extinction coefficient. It depends on how well the dipole caused by the electronic transition is aligned with the electric vector of the light wave. Because the intensity of the absorbance is related to the scalar product of both vectors, the maximum probability of absorption will occur when both are aligned at  $0^\circ$ , and the minimum will occur when both are orthogonal at  $90^\circ$ .<sup>26</sup> Combining all factors, the absorption ( $A$ ) at a given wavelength is governed by the Beer-Lambert law:

$$A(\lambda) = \epsilon(\lambda)cl$$

In solution, molecules don't absorb only specific wavelengths, but rather a range of wavelengths, seen by a broad Gaussian absorption peak (Figure 11). This is due mainly to the presence of smaller vibrational levels the electrons of each molecule in solution may be in. The difference in energy between these vibrational levels is much smaller than the difference in energy between electronic orbitals, resulting in a single broadened peak (Figure 11).<sup>26</sup>

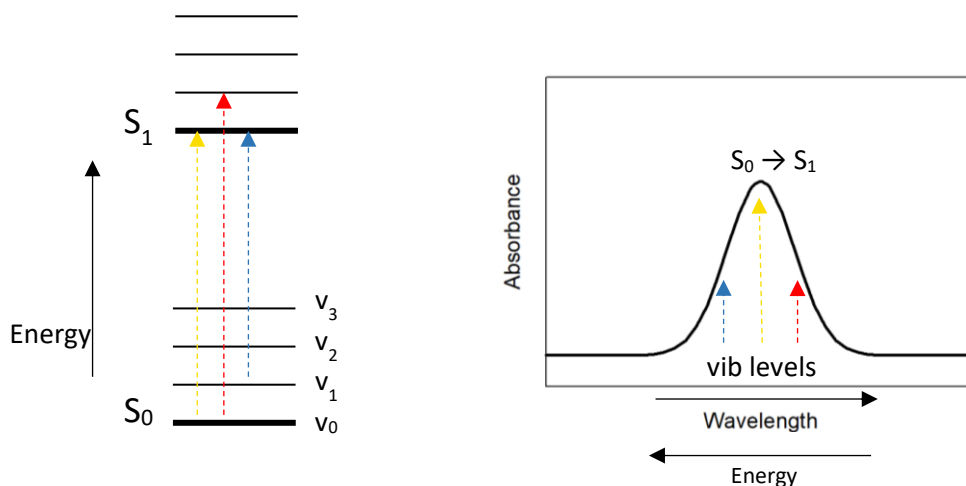


**Figure 11: Scheme of electronic transition with vibrational levels leading to a Gaussian-shaped peak in the absorption spectrum.**

### 2.3.2 Spectrophotometer

To measure the intensity of the absorption at any given wavelength, a spectrophotometer is used. At its simplest, it is composed of a light source capable of producing light in the UV, visible and near-infrared

range (from approximately 200 to 3000 nm) and a detector, which is often a photomultiplier tube. The detector converts the photons received into an electric current from the photoelectric effect. The absorbance is measured by comparing the intensity of light transmitted through the sample ( $I$ ) to the intensity of light originally shone onto the sample:  $A = \log_{10}\left(\frac{I_0}{I}\right)$ .<sup>26</sup>

Generally, the spectrometer also contains a monochromator, which is either a diffraction grating or a prism, to diffract or refract the light from the source into its different wavelengths, such that a specific wavelength can be selected to hit the sample by simply rotating the monochromator. In the case of a dual beam spectrophotometer, a beam splitter, which is a quickly rotating blade, is used to reflect a portion of light onto another sample, which is used as a reference cell. The absorbance is measured in the same way, using the intensity of light detected at the reference cell as  $I_0$  and the intensity of light measured at the sample cell as  $I$  (Figure 12).

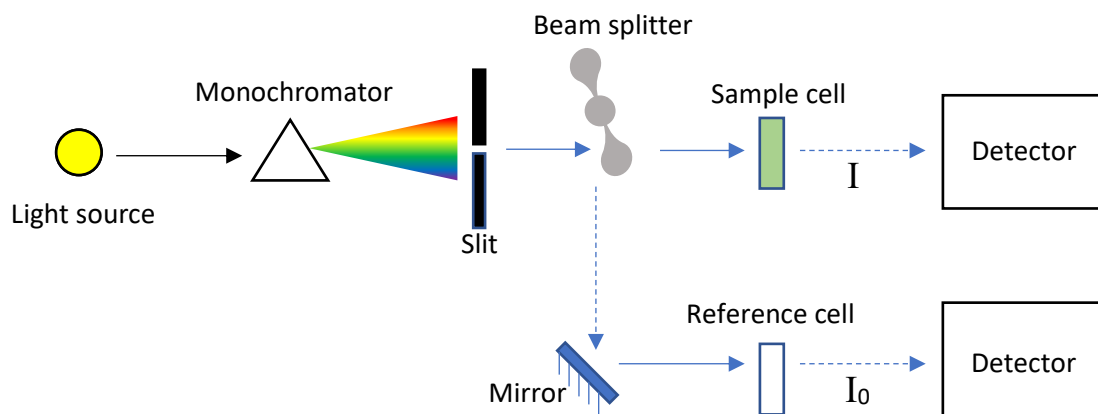


**Figure 12: Scheme of dual-beam absorbance spectrophotometer.**

### 2.3.3 Absorption Spectrum of the BRC

Bacterial reaction centre cofactors each have their own characteristic absorption peaks (Figure 13). The electron absorbs at longer wavelengths along the  $Q_y$  dipole of the porphyrin ring, so at lower energy, than along the  $Q_x$  dipoles. The peaks for the absorption along  $Q_y$  dipoles of the bacteriochlorophyll dimer, the monomers and the pheophytin cofactors are at 865 nm, 800 nm and 765 nm, respectively. The four chlorophyll molecules (the dimer and both monomers) have their  $Q_x$  absorption at around 600 nm, and the pheophytin absorbs in the  $Q_x$  dipole at slightly higher energy. Between 400 and 550 nm, the carotenoid has three nearby peaks. The Soret bands near 400 nm are characteristic peaks of all porphyrins. Last, the absorbance between 260 nm and 280 nm occurs from tryptophan, tyrosine and phenylalanine residues, and is found in virtually all proteins.<sup>27</sup>

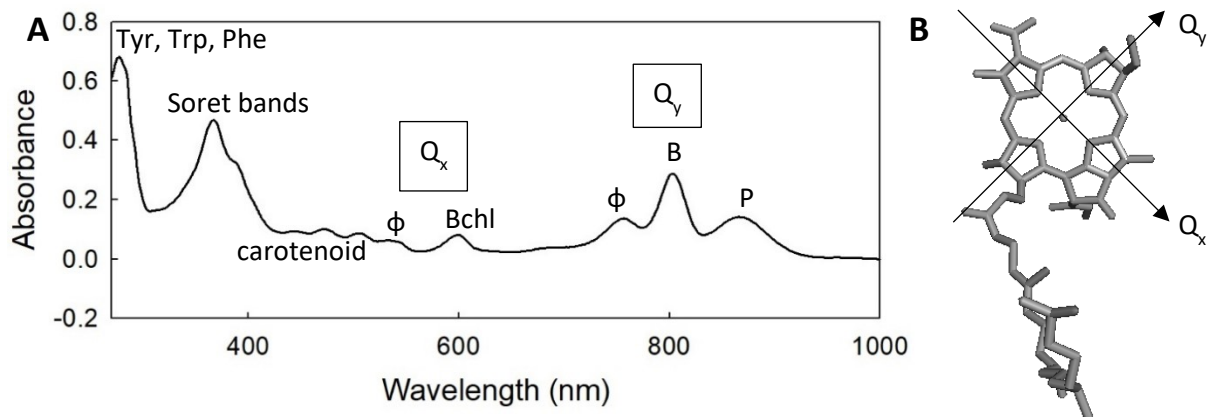


**Figure 13: (A) Full range (270 nm to 1000 nm) spectrum of wild-type reaction centre from *Rhodobacter sphaeroides*. (B)  $Q_x$  and  $Q_y$  dipoles on a porphyrin ring.**

In the light, an electron is transferred from the dimer. This causes the absorbance of the dimer to drop. The positive charge on the dimer will share an energetically unfavourable charge-dipole interaction with the dipole of the monomers. This causes the monomer peak to shift to higher energy. By the same principle, the negative charge on the quinone causes a shift to lower energies of the pheophytin peak.

To observe these changes, it is best to use difference spectroscopy. By subtracting the dark spectrum from the spectrum under illumination, small changes such as a shift or a band broadening can be observed. A shift in the spectrum, which is caused by a change in polarizability due to a change in the dielectric environment surrounding the molecule, is observed as a first derivative curve. A broadening or narrowing, caused by a change in the dipole, can be recognized by a second derivative curve, where the centre peak or trough is positioned at the same wavelength as the original peak.<sup>28</sup>

The light-minus-dark spectrum of the BRC can be decomposed to identify the changes experienced by the cofactors. It shows the oxidation of P as a Gaussian trough at 865 nm. The blue shift of the monomer is seen as a first derivative curve, with a peak below 800 nm and a trough above 800 nm. The red shift of the bacteriopheophytin is a smaller first derivative curve, in opposite orientation to the monomer shift (Figure 14).

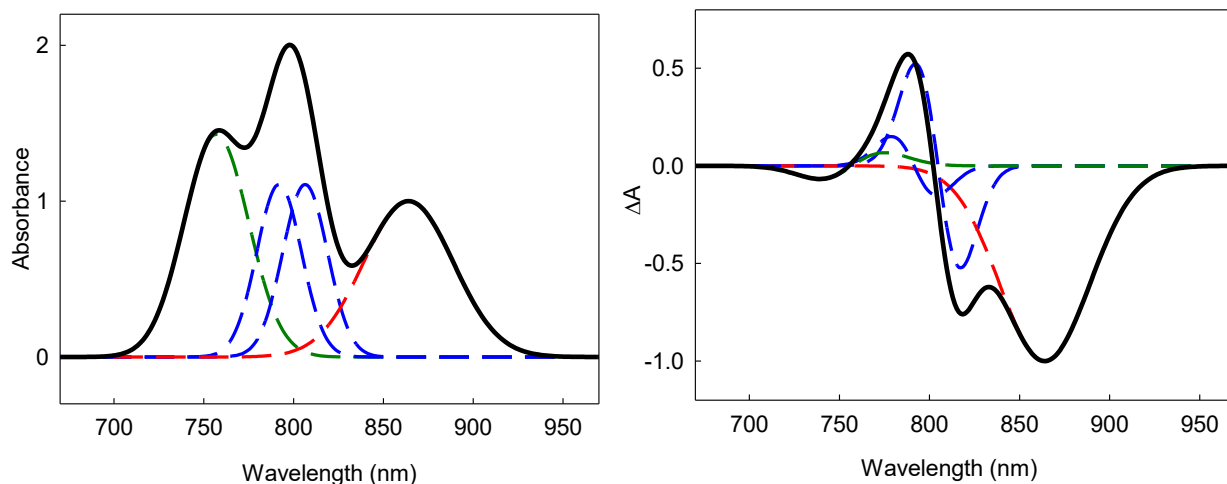


**Figure 14: (A) Model of NIR absorbance spectrum of BRC cofactors. Model of light-dark difference spectrum, with modeled changes in cofactor absorbances. Dimer in red, monomers A and B in blue, and pheophytin in green.**

#### 2.3.4 Optical Spectroscopy Experiments

All optical spectroscopy measurements were done using a Varian Cary 5000 Spectrophotometer, with an quartz-iodide visible source lamp, and deuterium UV source lamp. A baseline with 3 mL buffer in a quartz cuvette was measured at the start of each experiment. All experiments containing protein were done with 1  $\mu\text{M}$  BRC protein concentration. Protein was added to the buffer to obtain an OD800 of 0.28, with a 1 cm pathlength cuvette, corresponding to 1  $\mu\text{M}$  BRC concentration.

The external light source for the illumination of sample was a 250W tungsten lamp, product number EHJ JC24V-250W from Ushio, powered by a Sorenson DCS33-33E power supply. The total power of the lamp was set at 200 Watts, where approximately 1/3 of the BRC are  $\text{P}^+\text{Q}^-$  charge separated. The light was brought to the sample by a 7.6 mm wide liquid light guide from Newport, product code 77638.

#### *Absorbance Spectra*

Absorbance spectra were scanned at a range of 260 nm to 1000 nm at a rate of 2000 nm/min, when protein was present. Quartz-iodide visible light source was used for the whole range, with detector changeover at 650 nm. Without protein, the spectra were scanned from 260 nm to 650 nm at a rate of 2000 nm/min.

#### *Kinetics*

For the kinetics of the reaction of tetryl amplified by BRC, the difference spectra of the tetryl product with peaks at 350 nm and 415 nm were collected over time.

For the kinetics of the charge recombination, the absorbance at 865 nm was collected over time at intervals of 0.1 s. After zeroing and recording in the dark, the sample was illuminated with the external light source, at an intensity where approximately one third of the absorbance is lost, in other words, one third of the BRC is in the charge-separated state.

**Table 3: Solutions used for optical experiments.**

Buffer	Specifications	Product	Amount
pH 8 buffer	See TLE, 0.025% LDAO (Table 2)	Tris	10 mM
		LDAO	0.025 %
		EDTA	1 mM
pH 9.4 buffer	LDAO	bis-tris-propane	15 mM
		LDAO	0.025 %
		EDTA	1 mM
	triton	bis-tris-propane	15 mM
		triton TX-100	0.10 %
		EDTA	1 mM

## 2.4 Data analysis

Data from absorbance spectra or kinetic runs were manipulated and analysed using SigmaPlot 10, from Systat Software, Inc. Original files from the Cary spectroscopy software were imported onto SigmaPlot as .csv files.

### 2.4.1 Kinetics

#### *Product formation*

The kinetic trace of the formation of product from tetryl (Section 3.1.2) was drawn using the difference spectra collected. The absorbance at the wavelength corresponding to the maximum absorbance (peak) near 350 nm was plotted as a function of time. Plots obtained were fitted to exponential rise functions of type

$$f(x) = a(1 - \exp(-kx)) \quad (1)$$

where 'a' is the amplitude of the absorbance, representing the amount of product undergoing these kinetics, and 'k' is the rate constant, in s<sup>-1</sup> of the reaction. The traces were first attempted to be fit as mono-exponential, and if the R-squared obtained from the non-linear regression performed by the software showed a poor fit (generally less than 0.99) the traces were then fit to a bi-exponential function.

### Charge recombination

The charge recombination traces were first normalized so that the minimum absorbance, when the most BRC were charge-separated, was set to zero, and the maximum absorbance obtained when no more change in the absorbance was detected, several minutes after illumination, was set to 1 (when all BRC completed charge recombination). The traces representing the relative amount of charge-recombined BRC were then fit to di- or tri-exponential rise functions using Equation 1, where 'a' is the amplitude, the change in absorbance representing the relative amount of protein (between 0 and 1) in the conformational state undergoing these kinetics, and 'k' is the rate constant, in s<sup>-1</sup> of the reaction.

### Intermediate formation

For the fitting of the change in amplitude over time (Figure 27) of the charge-separated BRC with conformational changes around the dimer, or conformer C3 from Figure 9, two types of intermediate kinetic curves were used. First is the case of when only one intermediate is present, following the reaction scheme A → B → C of reagent A transforming into product C, via intermediate B, where the concentration of B is tracked. In this case, B represents the C3 conformer, and its the rate of change can be expressed as follows:

$$\frac{dB}{dt} = k_a[A] - k_b[B] \quad (2)$$

where k<sub>a</sub> and k<sub>b</sub> are respectively the rates of formation and disappearance of B. From the knowledge that the concentration of A follows a simple first-order decay of type  $[A] = [A]_0 e^{-k_a t}$ , and rearrangement of the terms, we can obtain the following equation:

$$\frac{dB}{dt} + k_b[B] = k_a[A]_0 e^{-k_a t} \quad (3)$$

This is a first order linear differential equation, that is generally represented by the equation

$$\frac{dy}{dx} + p(x)y = q(x) \quad (4)$$

with the general solution<sup>29</sup> of

$$y(x) = e^{-\int p(x)dx} \int q(x) e^{\int p(x)dx} dx + C e^{-\int p(x)dx} \quad (5)$$

When substituting the case where B<sub>0</sub> = 0, since no intermediate is present at time 0, we can obtain an expression for the integration constant, giving the entire formula for the concentration of B over time:<sup>30</sup>

$$[B] = \frac{k_a}{k_b - k_a} * (e^{-k_a t} - e^{-k_b t}) [A]_0 \quad (6)$$

The second type of intermediate used is in the case where the equation describes the concentration over time of the second of two intermediates. This would be used for monitoring the concentration of C over time, in the reaction scheme  $A \rightarrow B \rightarrow C \rightarrow D$ , where C is the amount of C3 conformers present. In this situation, we begin with the following differential equation to describe the rate of change of C:

$$\frac{d[C]}{dt} = k_b[B] - k_c[C] \quad (7)$$

The rate constants  $k_b$  and  $k_c$  describe the rate of formation and disappearance of C, respectively. We can replace [B] with Equation 6 and rearrange to obtain

$$\frac{d[C]}{dt} + k_c[C] = k_b * \frac{k_a}{k_b - k_a} * (e^{-k_a t} - e^{-k_b t})[A]_0 \quad (8)$$

Here,  $k_a$  is the rate of formation of B from A. Solving the same way as for the first intermediate case, the solution to the differential equation becomes:

$$[C] = \frac{k_a * k_b}{(k_b - k_a) * (k_c - k_b) * (k_c - k_a)} * ((k_c - k_b)e^{-k_a t} - (k_c - k_a)e^{-k_b t} + (k_c - k_b)e^{-k_c t})[A]_0 \quad (9)$$

#### 2.4.2 Spectral deconvolution

Absorbance spectra of the reaction centre and of the product were fit as a sum of Gaussian functions, of type

$$f(x) = a * \exp \frac{-((x-x_0)/b)^2}{2} \quad (10)$$

where a is the amplitude of absorbance of the peak, b is the standard deviation of the peak, and  $x_0$  is the peak position in nm.

Difference absorbance spectra of the reaction centre cofactors were fit to determine the source of the changes. Each cofactor's spectrum was fit as a difference of two Gaussians,

$$f(x) = a * \exp \frac{-((x-x_0)/b)^2}{2} - c * \exp \frac{-((x-z_0)/d)^2}{2} \quad (11)$$

where the second Gaussian term was set to the parameters obtained in the Gaussian fit for each cofactor previously described.

#### 2.4.3 Ligand binding curves

Sigmoidal curves were obtained either for the dependence of absorption peak position of picric acid on detergent concentration (Figure 20), the dependence of the components characterized by different rates of tetryl reaction on LDAO concentration (Figure 24), or for the dependence of the amplitudes of the

components characterized by different rate constants of charge recombination on the tetryl concentration (Figure 25). These curves were fit to ligand binding curve functions of the type

$$f(x) = \frac{A_0}{1 + \frac{x}{K_D}} + y_0 \quad (12)$$

where  $A_0$  is the maximum signal amplitude,  $y_0$  is the minimum signal amplitude, and  $K_D$  is the association/dissociation constant of the interaction. For cases where the sigmoidal curve was decreasing, the  $x/K_D$  fraction was inverted to  $K_D/x$ .

### 3 Results

This project began with the screening of the effect of different nitroaromatic explosives on BRC charge recombination. TNT, picric acid and tetryl, and some nitramine explosives were added at different concentrations to BRC. The charge recombination after a flash illumination was monitored to detect any changes in the kinetics. Because of their similarity in structure to DNOC, and because of the observed effect of TNT and picric acid on PSII,<sup>22,23</sup> it was expected that these explosives would also displace the secondary quinone and force the charge recombination to occur from  $Q_A$ , increasing the observed charge recombination rate after flash illumination.

The presence of TNT had no effect on the charge recombination up to 100  $\mu\text{M}$  concentration. Picric acid and tetryl, the other two nitroaromatic explosives screened, appeared to decrease the rate of charge recombination upon initial observation (Figure 15). The absorbance spectra of BRC in the presence of picric acid or tetryl were then recorded to more accurately characterize any effect seen. Only the absorbance spectrum of BRC in the presence of tetryl showed very distinguishable features (Figure 16). Tetryl was henceforth selected to undergo further analysis to optimize any effect seen and to understand the molecular mechanisms of the interaction.

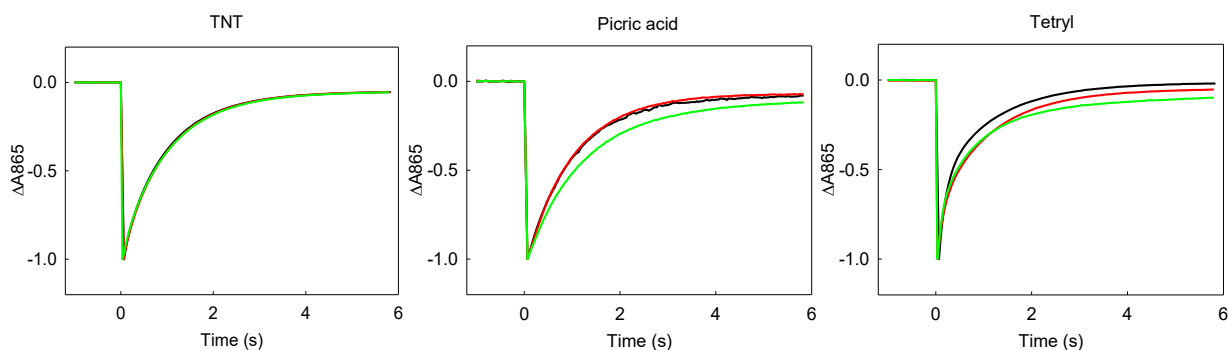


**Figure 15: Charge recombination kinetics after flash illumination of BRC in the presence of different nitroaromatic explosives. Black traces are in the absence of explosive, red traces are in the presence of 10  $\mu\text{M}$  explosives, and green traces are in the presence of 100  $\mu\text{M}$  explosives (or 60  $\mu\text{M}$  in the case of picric acid).**

#### 3.1 Tetryl product formation amplified by BRC

The interaction between tetryl and solubilized BRC in fact yields two observable effects as we will demonstrate: the protein amplifies the reaction between tetryl and detergent to yield a coloured product,

and the presence of tetryl slows the  $P^+Q^-$  charge recombination of the protein after illumination. We have investigated both effects to better understand the mechanism and location of the interaction.

### 3.1.1 Monitoring the coloured tetryl product formation: Absorbance spectroscopy

In this section, the absorbance spectrum of the product is studied for its possible use as a mode of detection for tetryl. It can also reveal information on the nature of the product and the environment it is in.

Upon addition of tetryl to BRC suspension containing LDAO detergent, a product with peaks at 345 nm and 415 nm is formed over time (Figure 16). The kinetics of the formation of the product can be measured by monitoring the change in absorbance at 345 nm over time. This will be explored in section 3.1.2. Additionally, the difference spectrum in the near-IR range shows changes in the spectra of the BRC cofactors. These changes represent differences in the energetics of the absorption, due to changes in the local environment caused by the association of tetryl or its reaction product with BRC.

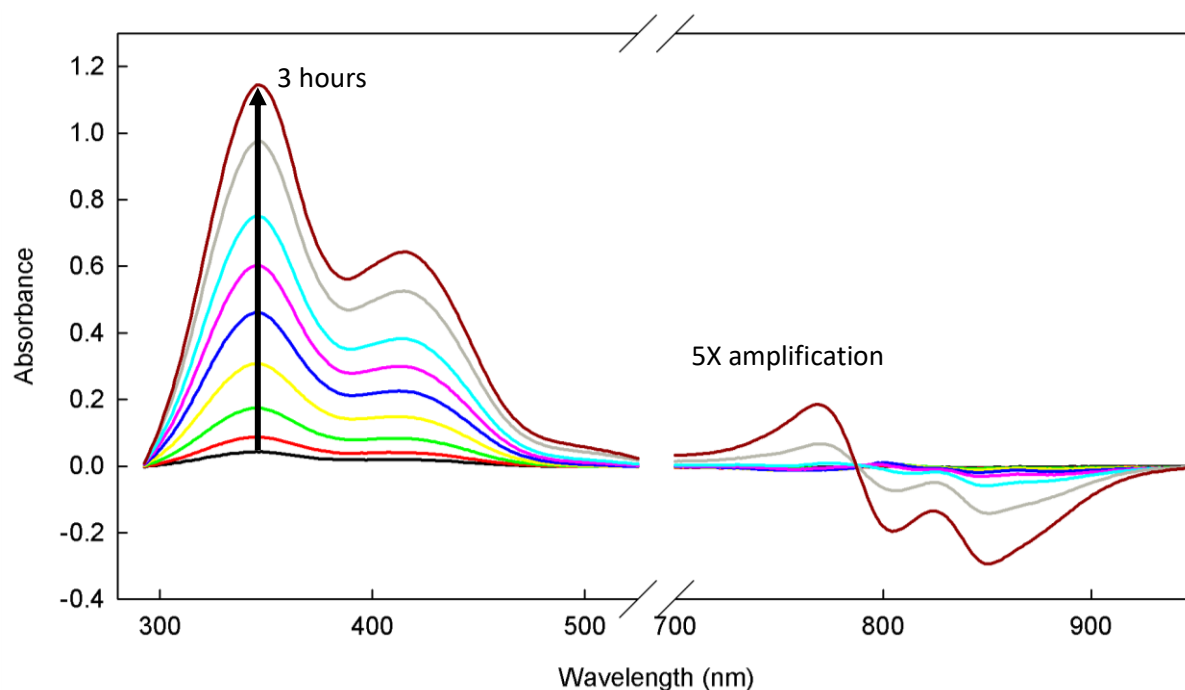


**Figure 16: Product formation resulting from the addition of tetryl to BRC in the dark. Different coloured traces show the emergence of peaks at 345 nm and 415 nm over time, and the changes of the BRC forming over time. NIR range (700-1000 nm) was amplified by 5-fold to show features. 100  $\mu$ M tetryl were added to 1  $\mu$ M R26 BRC at pH 9.4, with 0.025% LDAO.**

The change in the spectrum of the BRC cofactors occurs in the dark after addition of tetryl. The changes are best modeled as a blueshift of B<sub>B</sub>, which is the monomer in the cavity in the M subunit, which contains the carotenoid, and a bleach of the dimer (Figure 17A). Alternatively, the changes can also be fit as a broadening of B<sub>A</sub>, the monomer in the cavity without the carotenoid, and a bleach and redshift of the dimer (Figure 17B). Thus, these differences are quantitatively distinct from those that occur upon illumination of BRC, see Section 2.3.3

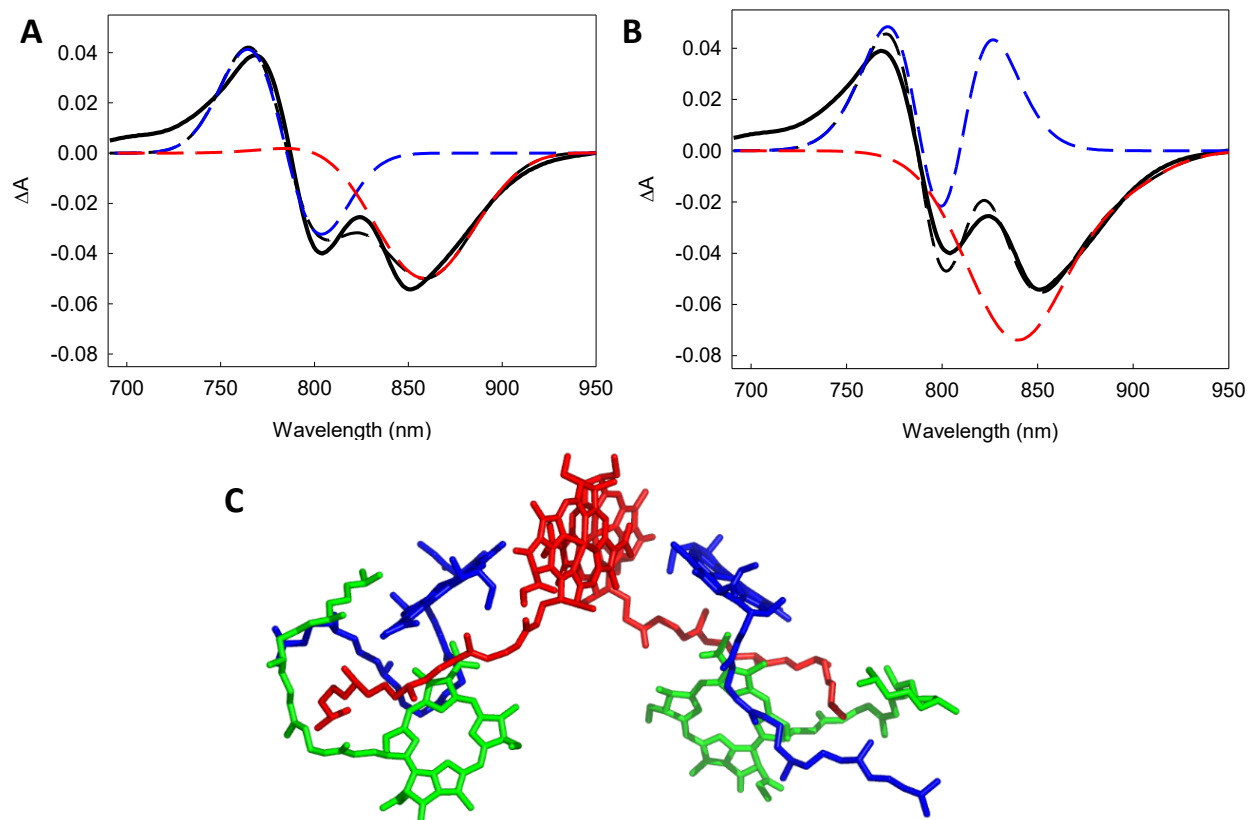


**Figure 17: Change in the environment of cofactors of the BRC in the presence of tetryl. (A-B) Difference spectrum of BRC cofactors (black) obtained 3 hours after tetryl addition. The spectrum was decomposed into different electrochromic absorption changes assuming interactions between the bound tetryl or its product and the cofactors, with Gaussian difference fits for both monomer and dimer (dashed black), of type  $f(x) = a * \exp\left(\frac{((x-x_0)/b)^2}{2}\right) - c * \exp\left(\frac{((x-z_0)/d)^2}{2}\right)$ . (A) Difference of Gaussian fits for a 7-nm blueshift in monomer B (dashed blue) and 30 % loss of absorbance of dimer (dashed red). (B) Difference of Gaussian fits for a broadening in monomer A, by an increase by 4 nm of the FWHM (dashed blue) and an 8-nm redshift and 35 % loss of absorbance of dimer (dashed red). (C) Pymol structure of cofactors involved in NIR absorbance: at pH 9.4, bacteriochlorophyll dimer (red) absorbs at 855 nm,**

**bacteriochlorophyll monomers A and B (blue) absorb at around 800 and 783 nm respectively, and bacteriopheophytin (green) absorbs around 755 nm.**

The formation of product has been found to occur even in the absence of protein. When tetryl is added to the buffer containing LDAO, the product still forms gradually over time. The product formation is amplified by the presence of protein. After an hour incubation of tetryl with R26 strain protein and 0.025 % LDAO, there is an observed 30-fold stronger signal than with LDAO alone. When investigating lower concentrations in order to estimate the limit of detection, it was found that the signal generated at 350 nm after 500 nM of tetryl reacted for an hour in the presence of protein gave a signal-to-noise ratio of around 5. The noise was calculated as the difference between the maximum and minimum absorbance over the range recorded, and the signal was the absorbance recorded at 350 nm. This concentration would be a tentative limit of detection, under the conditions of pH 9.4 with 0.025% LDAO and 1  $\mu$ M R26 BRC (Figure 18). The noise appears to increase over lower wavelengths. If the absorbance peak at 420 nm is used, which is lower at higher concentrations of tetryl, but appears in a 1:1 ratio with the 350 nm absorbance peak when 500 nM tetryl is used, it seems possible to detect even lower tetryl concentrations.

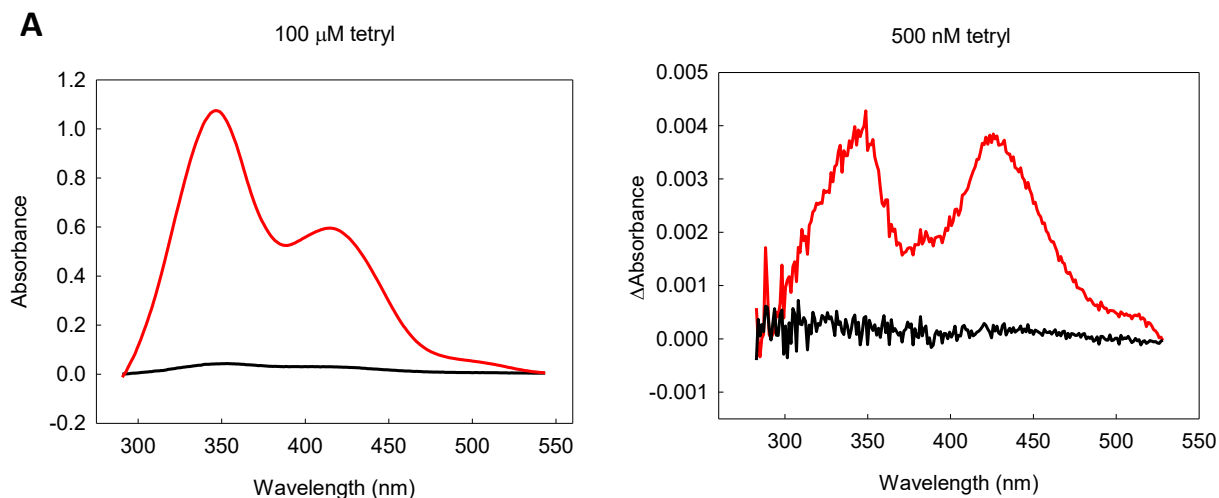


**Figure 18: The presence of the solubilized protein amplifies the detection of tetryl. (A) Product formation in the presence (red) and absence (black) of the R26 protein, with 0.025 % LDAO at pH 9.4, after 1 hour. (B) Signal of product formation of 500 nM tetryl with R26 protein (red), compared to the noise of the spectrophotometer (black), with 0.025 % LDAO at pH 9.4, after 1 hour.**

The spectrum of the product generated at pH 9.4 when tetryl was added to BRC is similar to that of picric acid, a known hydrolysis product of tetryl.<sup>31</sup> Upon closer inspection, when tetryl is in the presence of low LDAO concentration (0.025%), the lower wavelength peak is 5 nm blueshifted with respect to the

equivalent peak of picric acid in the same environment (Figure 19A). In the presence of R26 strain of the BRC, the spectrum matches that of the product of tetryl in the presence of LDAO at the same concentration without protein.

To see whether the product is specific to zwitterionic LDAO, tetryl was added to solution containing non-ionic Triton-X100 (TX-100, Triton) detergent. Even with Triton, a product is formed, but with slightly different peaks. In the presence of 0.1% TX-100 at pH 9.4, tetryl also does not hydrolyse into picric acid, as both spectrum peaks of the product are 5 nm lower in wavelength than those of the picric acid in the same buffer (Figure 19B). In the presence of R26 strain BRC, the spectrum of the product of tetryl with 0.1% TX-100 matches that of the spectrum of the tetryl product with TX-100 in 5% detergent without BRC.

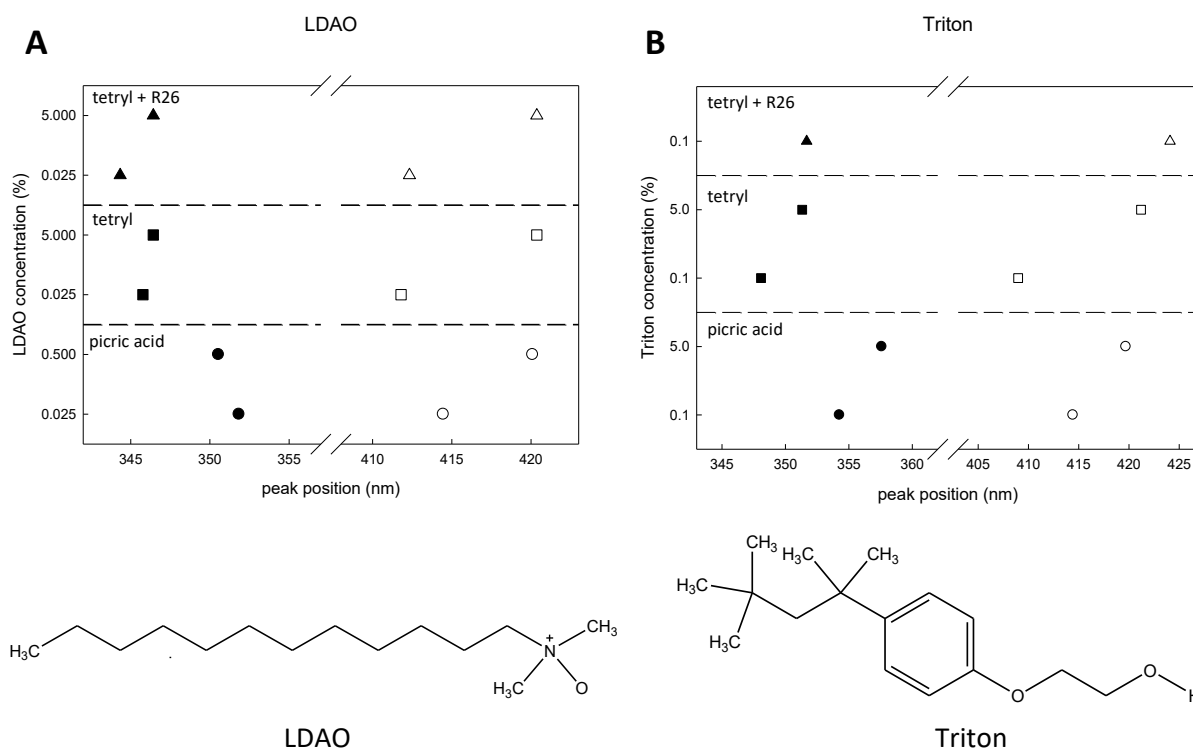


**Figure 19: Different tetryl products are formed with different detergents. Peaks of product formed with tetryl in the presence or absence of R26-strain protein, with different detergent concentrations, were estimated by a gaussian fit and compared to the peaks of picric acid in the same solution. (A) LDAO detergent (B) Triton-X100 detergent.**

The environment of the absorbing electron can impact the absorbance spectrum in many ways, some of which are described in Section 2.3 The spectrum of picric acid was taken with increasing concentrations

of LDAO or TX-100 detergent, to determine the extent of the effect of the environment on picric acid, and to investigate whether the product from tetryl and detergent could be picric acid in a different environment.

The spectrum peaks of picric acid, like the peaks of the tetryl product, shift depending on which environment they are in. When the concentration of LDAO is increased, the bluer peak shifts to a shorter wavelength, whereas the redder peak shifts to a longer wavelength. The association constant ( $K_D$ ) for the process was found at around 1 mM LDAO (0.8 mM and 1.7 mM for the first and second peaks, respectively). In increasing triton concentration, both peaks are redshifted (Figure 20). For this process, the  $K_D$  was fitted at around 7 mM and 9 mM for the first and second peaks, respectively. Over the range of the concentrations shown in Figure 20, no shift caused by the detergent concentration could cause the picric acid absorbance spectrum to match the tetryl product spectra in either detergent. Thus, our product(s) are likely not picric acid, but some other, similar compound(s).

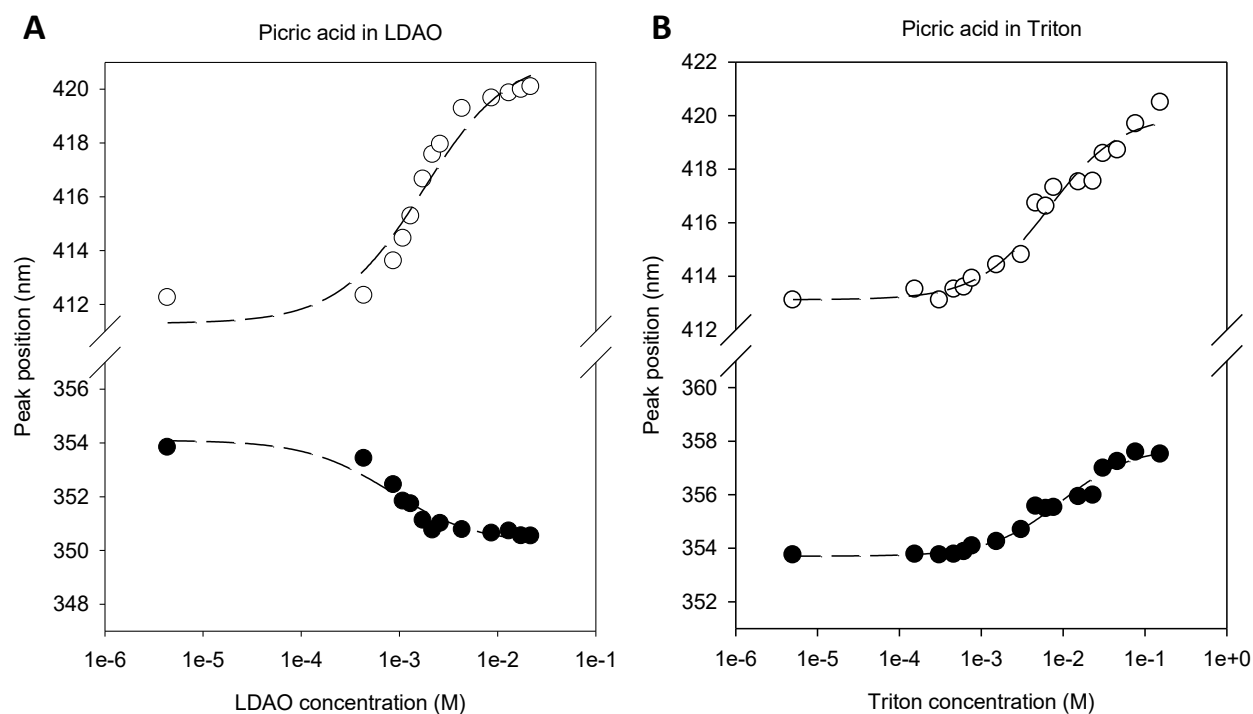


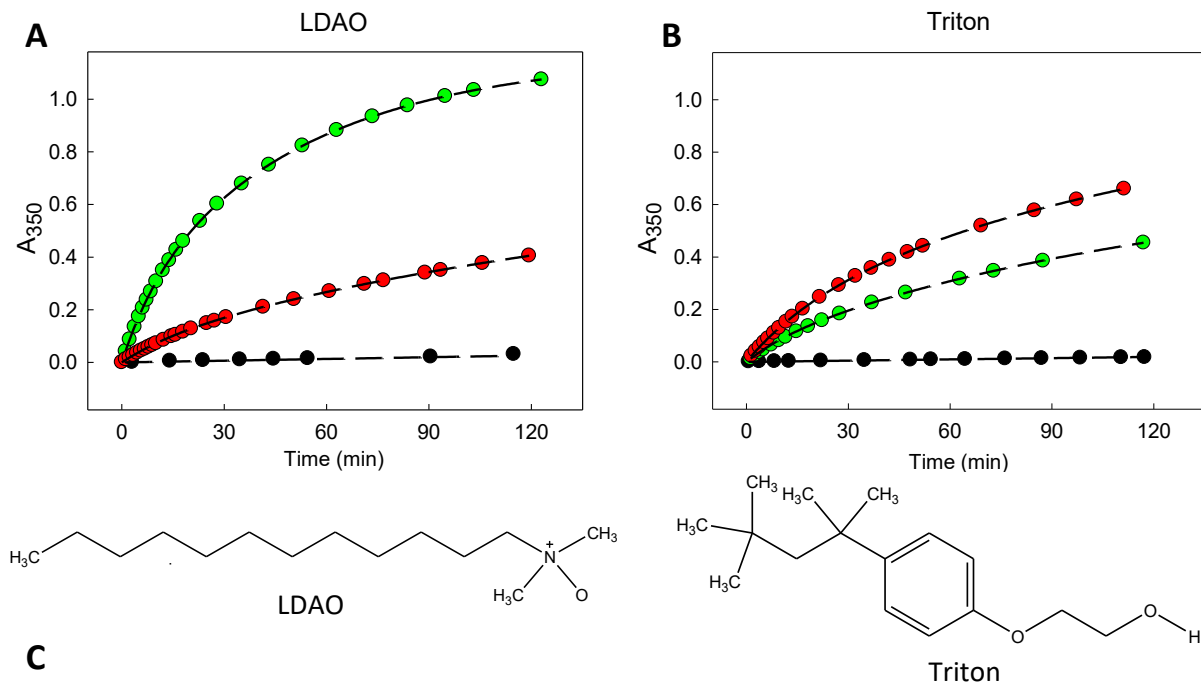
**Figure 20: Picric acid peak positions are dependent on the dielectric properties of the environment. Picric acid peaks in (A) LDAO detergent, (B) in Triton-X100 detergent. Traces were fit to binding kinetics of type  $f(x) = A_0/(1 + \frac{x}{K_D})$ , where  $K_D$  is the association/dissociation constant of the interaction.**

### 3.1.2 Kinetics of product formation

In this section, the kinetics of the product formation are measured in different conditions. Finding the optimal set of conditions will help amplify the signal for use in the optical detection of tetryl and can also help elucidate the mechanism and location of the reaction.

The kinetics of the reaction of tetryl in the presence of 0.025% LDAO without protein follows a monoexponential rise function with a rate constant of  $2.0 \times 10^{-4} \text{ min}^{-1}$ . In the presence of Wild-Type (WT) protein, the component following this small rate constant can still be observed. However, in WT, a new, 80-fold faster component can also be detected with a rate constant of around  $1.6 \times 10^{-2} \text{ min}^{-1}$ . In the carotenoid-less R26 strain, the reaction is faster and thus, the component found in the absence of protein is no longer visible. The second component found in WT is present, along with a third, even faster component with a rate constant of  $7.7 \times 10^{-2} \text{ min}^{-1}$ . This component is 5-fold faster than the one also found in WT and can only be seen if LDAO is used as the detergent (Figure 21A).

When the LDAO detergent is replaced with TX-100, the bulk rate and slower of the protein-specific rates are nearly the same as when LDAO is used. The fastest component cannot be observed suggesting there are three different kinds of LDAO molecules that react with tetryl, location-wise, whereas there are only two types of TX-100 molecules. One kind is unbound to protein, either in an empty micelle or in the bulk, another is bound in the hydrophobic cavity of BRC, and the third is specifically bound to the carotenoid binding site. If TX-100 is used, LDAO from the carotenoid binding site diffuses out of the cavity due to lower LDAO concentrations, and as a result only the two slower kinetic components can be detected (Figure 21B). The combination of these three reaction locations give rise to the overall observed 30-fold amplification seen in Figure 18.

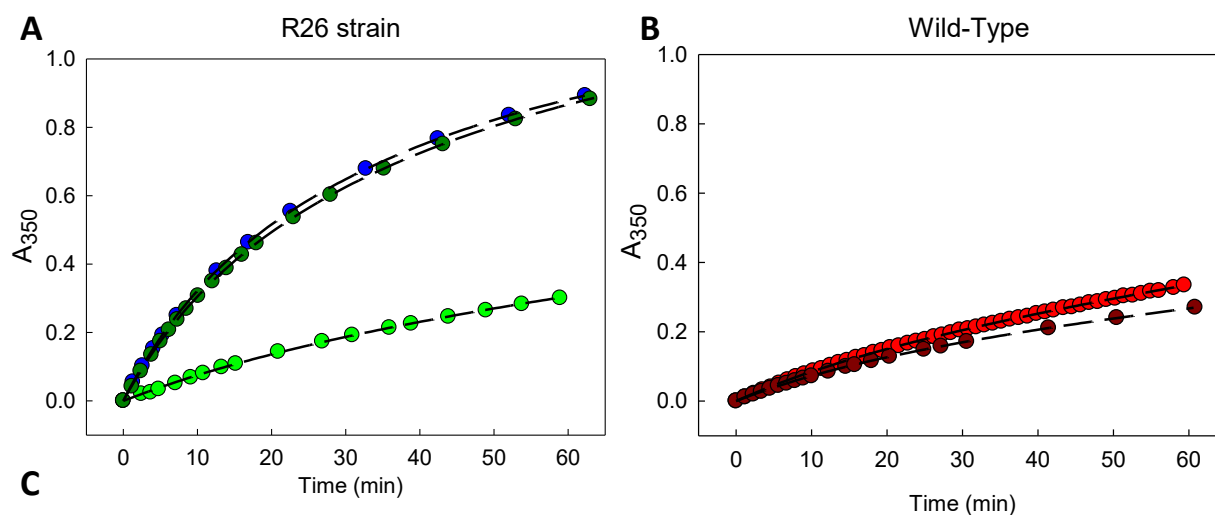


		a1	k1 ( $\times 10^{-4} \text{ min}^{-1}$ )	a2	k2 ( $\times 10^{-2} \text{ min}^{-1}$ )	a3	k3 ( $\times 10^{-2} \text{ min}^{-1}$ )
LDAO	buffer	1.14	1.95				
	WT	0.97	1.95	0.43	1.60		
	R26			0.88	1.60	0.33	7.69
Triton	buffer	1.13	1.43				
	WT	0.78	1.43	0.72	1.86		
	R26	1.00	1.43	0.50	1.63		

**Figure 21: Detergent and BRC strain specificity, pH 9.4. Kinetics of tetryl reaction without protein (black), with WT BRC (red) or with R26 strain BCR (green), in the presence of A) 0.025% LDAO, B) 0.1% TX-100. C) Table with amplitudes of components and rate constants. Fits were done with exponential rise functions describing the emergence of product at 345 nm. For buffer, a monoexponential fit was used, a biexponential fit was used for WT and R26 reaction kinetics.**

The illumination state of the protein affects the kinetics of the tetryl-LDAO reaction. Under our particular illumination conditions, about 80-90% of the hour-long illuminated protein are charge-separated  $P^+Q^-$ . Pre-illuminated proteins no longer have charges, but a portion of the population will remain in the conformational state associated with longer-lived charge separation for several hours after the illumination. Only up to 20% of the sample had the charge recovering with a rate constant of around  $1 \text{ s}^{-1}$ , meaning at least 80% of the sample was in some light-induced conformationally altered state.

The formation of the product in the presence of the light-induced conformation of the R26 BRC protein has nearly identical reaction kinetics as when the protein is completely dark-adapted. The reaction with illuminated R26 sample shows kinetics similar to the reaction with Wild-Type strain, independent of the illumination state of the Wild-Type sample. The fast rate of  $7.7 \times 10^{-2} \text{ min}^{-1}$  specific to R26 is no longer present in light while illuminated (Figure 22).

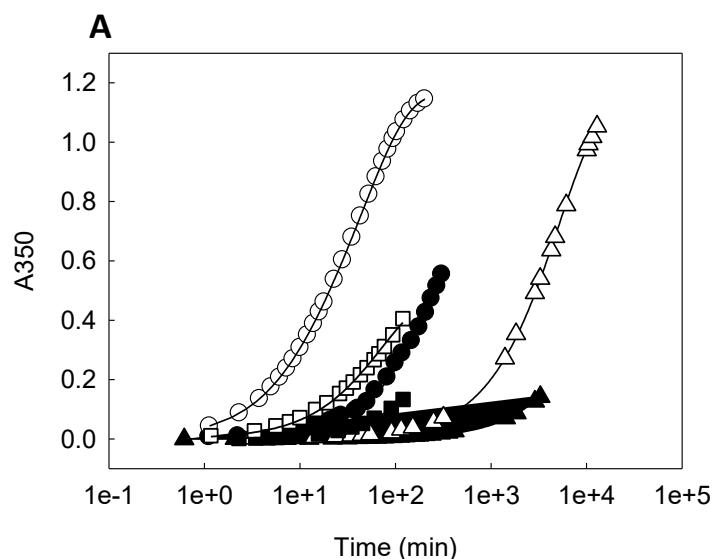


		<i>a1</i>	<i>k1</i> ( $\times 10^{-4} \text{ min}^{-1}$ )	<i>a2</i>	<i>k2</i> ( $\times 10^{-2} \text{ min}^{-1}$ )	<i>a3</i>	<i>k3</i> ( $\times 10^{-2} \text{ min}^{-1}$ )
<b>R26</b>	<i>dark</i>			0.88	1.60	0.33	7.69
	<i>pre-illuminated</i>			0.79	1.60	0.39	7.69
	<i>illuminated</i>	1.00	1.95	0.50	1.60		
<b>WT</b>	<i>dark</i>	0.97	1.95	0.43	1.60		
	<i>illuminated</i>	0.88	1.95	0.52	1.60		

**Figure 22: Effect of illumination of protein. (A) Kinetics of tetryl-LDAO reaction with different illumination states of R26 strain, dark green: dark, blue: pre-illuminated, light green: illuminated. (B) Kinetics of tetryl-LDAO reaction with different illumination states of WT strain, dark red: dark, light red: illuminated. (C) Table with biexponential fits. Rate constants were determined by the fits from mono or biexponential rise functions. Runs were done with 1  $\mu\text{M}$  BRC, 100  $\mu\text{M}$  tetryl and 0.025% LDAO.**

The pH influences the reaction kinetics. At pH 8, without protein, the reaction occurs with a rate constant 10-fold slower than at pH 9.4. In the presence of protein, the kinetic components at pH 8 are qualitatively the same as for pH 9.4, except with overall slower rates. With the R26 strain, the reaction gives a biexponential rise with two rate constants, one about 5-fold faster than the other (around  $6.5 \times 10^{-3} \text{ min}^{-1}$  and  $1.5 \times 10^{-3} \text{ min}^{-1}$ ). In Wild-Type, only the slower rate from the R26-amplified reaction is present. In

buffer, the rate is two orders of magnitude slower than in the presence of protein, around  $4.3 \times 10^{-5} \text{ min}^{-1}$ .<sup>1</sup> All rates at pH 8.0 are around 10-fold slower than the corresponding rates at pH 9.4 (Figure 23).



**B**

sample		a1	k1	a2	k2	a3	k3
			( $\times 10^{-4} \text{ min}^{-1}$ )		( $\times 10^{-2} \text{ min}^{-1}$ )		( $\times 10^{-2} \text{ min}^{-1}$ )
pH 8	Buffer	1.10	0.43				
	R26			0.95	0.15	0.24	0.64
	WT			1.10	0.11		
pH 9.4	Buffer	1.14	1.95				
	R26			0.88	1.60	0.33	7.69
	WT	0.97	1.95	0.43	1.60		

**Figure 23: pH dependence of tetryl reaction with 0.025% LDAO. (A) Kinetic traces of the change in absorbance versus time in a logarithmic scale to show slower reactions. Open symbols are runs at pH 9.4, and black symbols are at pH 8.0. Circles are in the presence of R26 BRC, squares are in the presence of WT BRC, triangles are in buffer alone.**

The kinetics of the reaction between tetryl and LDAO are biexponential at higher concentrations of LDAO, even in the absence of protein (Figure 24). There is a component ( $a_1$ ) with a slow rate constant of around  $2.0 \times 10^{-4} \text{ min}^{-1}$  when 0.025 % LDAO is used, and another component ( $a_2$ ) with a faster one in the range of  $10^{-2} \text{ min}^{-1}$ , two orders of magnitude faster than the slow one.

The relative amount of tetryl reacting with the fast rate constant increases while the amount reacting more slowly decreases as more LDAO is added, as demonstrated by the changes in the amplitudes of the

exponential fits in Figure 24A. Additionally, the rate constants appear to increase linearly with the concentration of LDAO, indicative of second order collisional reactions.

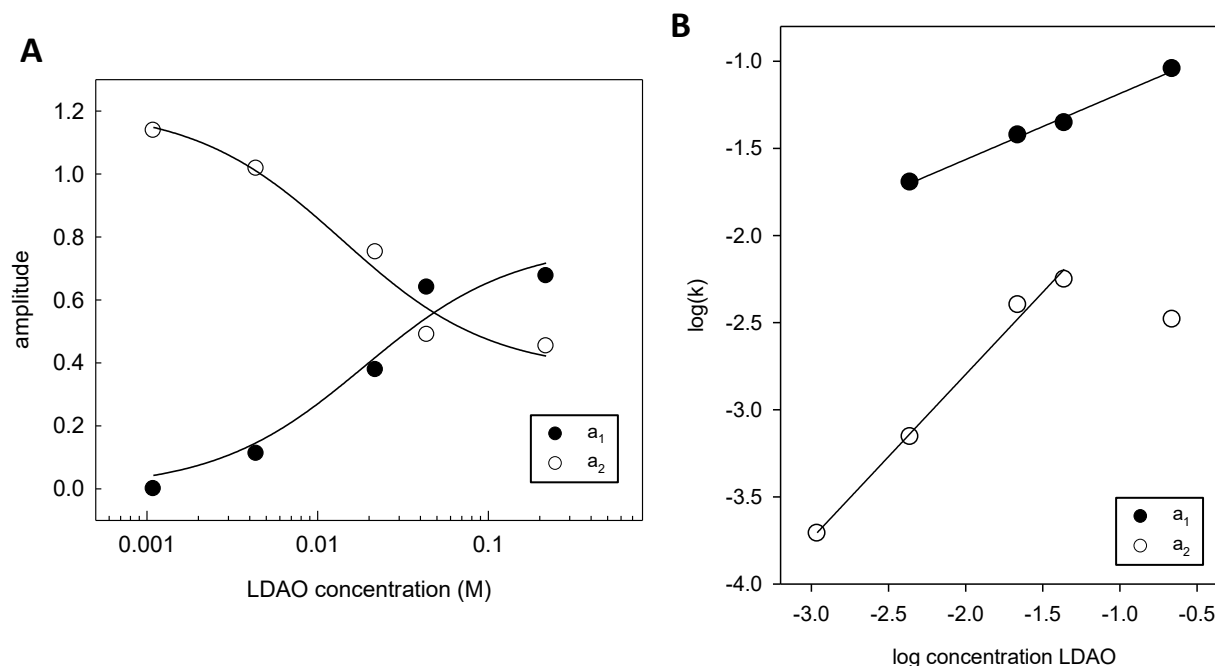


**Figure 24: LDAO concentration dependence on tetryl reaction kinetics, pH 9.4. The formation of product was fit to mono or biexponential rise functions of type  $f(x) = a(1 - \exp(-kx))$ , where  $a$  is the amplitude, or population of product evolving at a given rate constant,  $k$ . (A) Plot of amplitudes of both rate constants over time. Plots were fit to binding kinetics of type  $f(x) = \frac{A_0}{1 + \frac{x}{K_D}}$ , where  $K_D$  is the association/dissociation constant of the interaction. (B) Plot of  $\log(k_1)$  (faster rate constant) and  $k_2$  (slower rate) versus  $\log$  of molar concentration of LDAO, fitted with a linear regression.**

In the presence of BRC, the relative amplitudes of the kinetic components are dependent on the concentration of tetryl added, suggesting a binding interaction. In the presence of 10  $\mu\text{M}$  tetryl, the rate follows a mono-exponential rise function: there is only the slower protein-dependent rate constant (around  $1 \times 10^{-2} \text{ min}^{-1}$ ). The faster protein-dependent rate constant (around  $5 \times 10^{-2} \text{ min}^{-1}$ ) only becomes apparent at higher tetryl concentrations. At 50  $\mu\text{M}$  tetryl, approximately 15 % of the tetryl reacts with the higher rate constant, and at 100  $\mu\text{M}$  tetryl, over 25 % reacts with the higher rate constant. Over this concentration range, the relative amplitude of the fast protein-dependent rate constant increases as the tetryl concentration increases (Figure 25).

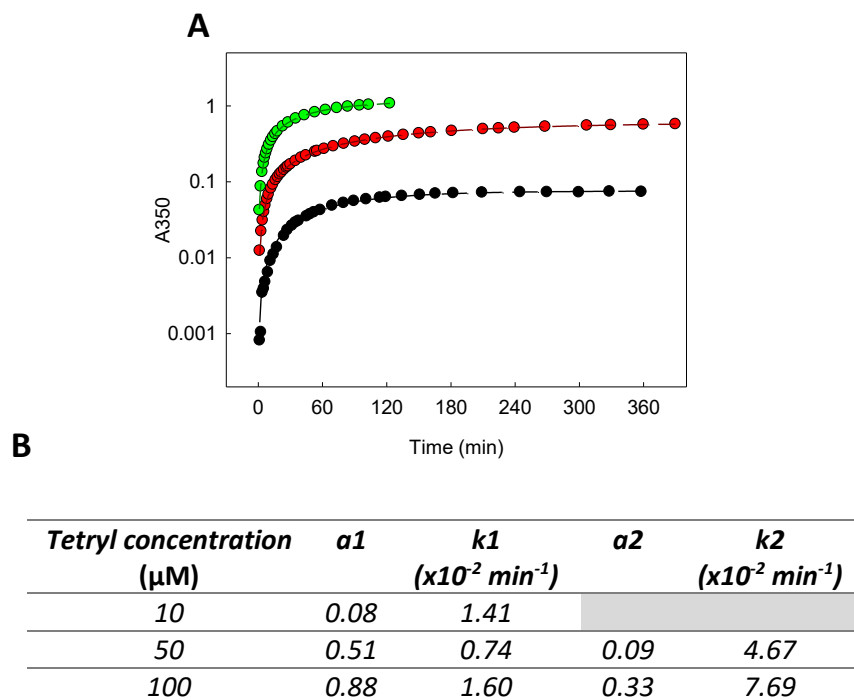


**Figure 25: Tetryl concentration dependence on the protein-amplified reaction kinetics. (A) 10  $\mu\text{M}$  tetryl (black), 50  $\mu\text{M}$  tetryl (red), 100  $\mu\text{M}$  tetryl (green). (B) Table of kinetic parameters of concentrations shown. Runs were at pH 9.4, with 1  $\mu\text{M}$  R26 BRC, 0.025% LDAO.**

### 3.2 Effect of tetryl on BRC charge recombination kinetics

The charge recombination kinetics of BRC in the presence of tetryl are studied in this section. Changes in the kinetics could be used as an electrochemical detection mode in a biosensor. Additionally, these changes could provide more insight on the mechanism of the interaction for further optimizing the biosensing potential of the protein, and for the eventual design of biologically-inspired light-activated charge storage devices.

Originally, the tetryl was expected to have a similar role to DNOC, a nitroaromatic compound that acts as a herbicide. By binding to the ubiquinone B binding site, DNOC blocks the electron transfer to this cofactor to inhibit photosynthesis. In vitro, this inhibitor increases the charge recombination rate constant observed, since the recombination must take place from  $Q_A$  with faster kinetics.<sup>19</sup>

Contrarily to this hypothesis, the addition of tetryl slows the observed charge recombination by increasing the population of the protein that recovers with a slow rate of  $10^{-2} \text{ s}^{-1}$ , matching the long-lived charge recombination caused by light-induced conformational changes near the dimer, referred to as C3

conformer (Figure 9).<sup>13-15</sup> The stable rate constants as tetryl concentration increases indicate the mechanism is a first order binding process between tetryl and the protein, with a  $K_D$  of around 60  $\mu\text{M}$  (Figure 26).

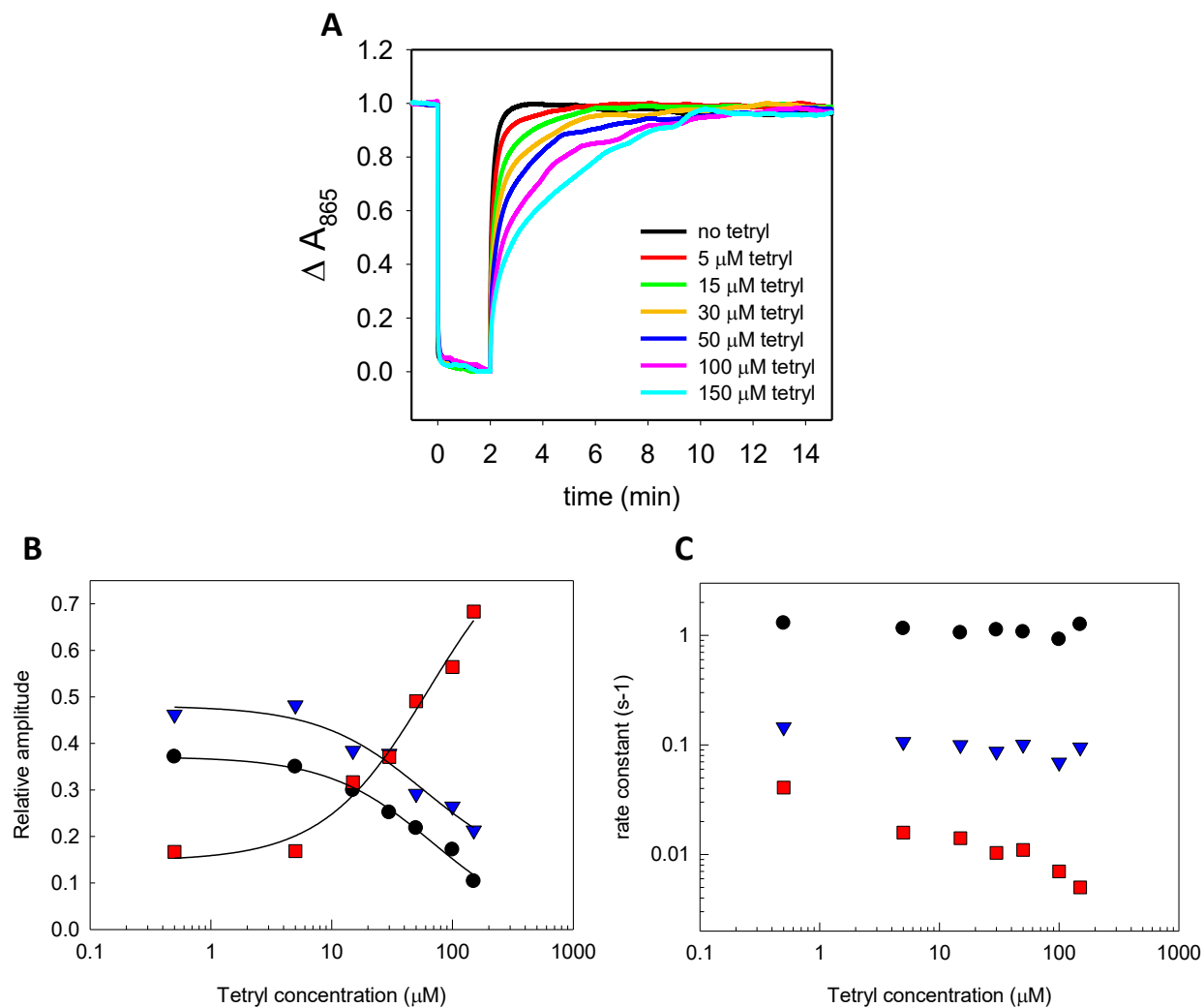


**Figure 26: Effect of tetryl concentration on BRC charge recombination, pH 8.0. (A) Charge separation and charge recombination of R26 strain BRC in the presence of tetryl at different concentrations. Charge recombination curves were fit as triexponential functions. (B) Amplitudes of different exponential components. Plots were fitted with sigmoidal binding curves of type  $f(x) = A_0 / (1 + \frac{x}{K_D})$ , where  $K_D$  is the association/dissociation constant of the interaction. (C) Rate constants of different exponential components associated to the different conformers: dark-adapted conformer (C1) in black, Q-site conformer (C2) in blue and P-site conformer (C3) in red.**

The effect of tetryl on the charge recombination kinetics changes as a function of the time tetryl was incubated with the protein in the dark. At pH 8, over the first 3.5 hours, the amount of C3 conformer (Figure 9) long-lived charge-separated protein with a charge recombination rate constant of  $0.01 \text{ s}^{-1}$  increases gradually. If the protein is left in the dark with tetryl for longer before illumination, we begin to see a decrease in the amount of charge-separated proteins that recover with the slower rate constant.

The curve of the relative amplitude of the C3 conformer was first fit to the equation dictating the amount of intermediate present over time. This would imply that there is a rate constant associated to the formation of the charge-stabilized conformation of around  $6 \times 10^{-3} \text{ min}^{-3}$ , and of  $5.2 \times 10^{-3} \text{ min}^{-3}$  for the return to the dark-adapted conformation C1. However, the fit for the second intermediate kinetics over time gave a better fit (R-squared of 0.89 for the second intermediate fit versus R-squared of 0.80 for the first intermediate fit). This suggests that there are two consecutive steps leading to the formation of the long-lived charge-separated state with a charge recombination rate constant of  $0.01 \text{ s}^{-1}$ . In this case, all rate constants are in the  $10^{-2} \text{ min}^{-1}$  range.

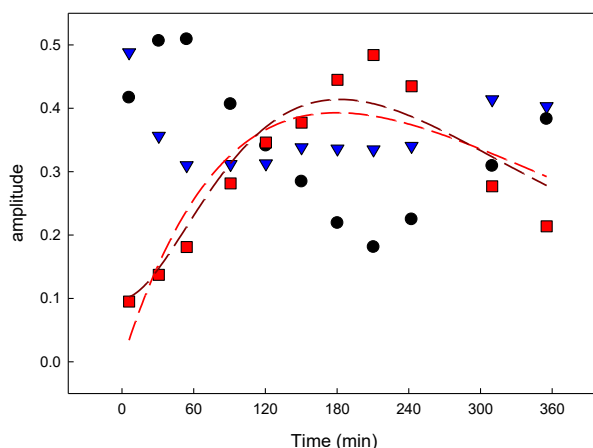


**Figure 27: Effect of tetryl incubation time on long-lived charge separated state at pH 8.0. Relative amplitude of different exponential components of the charge recombination of R26 BRC in the presence of tetryl, with different incubation times. Red: amplitude of the C3 conformer, the longest-lived charge separated state with a rate constant of  $0.01 \text{ s}^{-1}$ . Fit to the exponential  $f(x) = a * \left(\frac{b}{a-b}\right) * (exp(-bx) - exp(-dx))$ , for intermediate reactions is in red dash, where b and d are rate constants for the formation and disappearance of the intermediate, respectively. Fit to the case where the long-lived charge separated conformation is a second intermediate, following the equation:**

$f(x) = a * \frac{b*d}{(d-b)*(g-b)*(g-d)} * \exp((g - d) * \exp(-bx) - (g - b) * \exp(-dx) + (d - b) * \exp(-gx))$  is in dark red dash, where b and d are the rates of formation and disappearance of the first intermediate, and g is the rate of disappearance of the second intermediate (see Section 2.4.1 Blue: amplitude of rate constant of  $0.1 \text{ s}^{-1}$ , corresponding to charge recombination rate of C2 conformer, with conformation changes of  $Q_B$ . Black: amplitude of rate constant of  $1 \text{ s}^{-1}$ , corresponding to charge recombination rate in C1 conformer dark-adapted protein.

When BRC is incubated with tetryl at pH 9.4, where the observed rate of product formation is higher, the effect of tetryl is lower. Only about 10% of the sample is observed to be in long-lived charge-separated state, with a rate constant of  $0.01 \text{ s}^{-1}$  initially. After 2 hours of incubation time in the dark, there is no longer any protein with  $0.01 \text{ s}^{-1}$  charge recombination rate constant, and after 4 hours, the sample has the same kinetics as in the absence of tetryl (Figure 28).

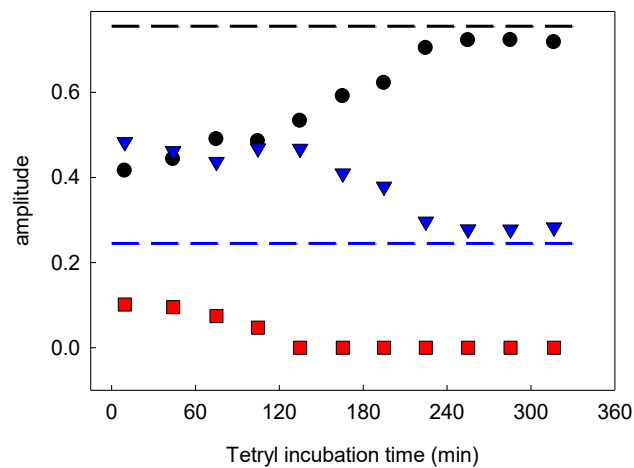


**Figure 28: Effect of tetryl incubation time on BRC long-lived charge separated state at pH 9.4. Relative amplitude of different exponential components of the charge recombination of R26 BRC in the presence of tetryl, with different incubation times. Red: amplitude of long-lived charge separated state rate constant of  $0.01 \text{ s}^{-1}$ . Blue: amplitude of rate constant of  $0.1 \text{ s}^{-1}$ , corresponding to charge recombination rate in light-adapted protein. Black: amplitude of rate constant of  $1 \text{ s}^{-1}$ , corresponding to charge recombination rate in dark-adapted protein. Dashed lines represent amplitudes of respective rate constants when no tetryl is present.**

Without tetryl, the charge recombination kinetics are slower at pH 8. The light and dark-adapted conformations are present at approximately a 1:1 ratio (Figure 27). At pH 9.4, without tetryl, there is nearly 80% of the dark-adapted protein.

The largest effect of tetryl on the charge recombination kinetics of BRC is seen at pH 8. Almost 70 % of the protein recovers with the slowest rate constant after only 2 minutes illumination. At pH 9.4, there is only up to 10 % of the population that recovers with the slowest rate constant. The incubation time also does not have the same effect at both pH levels. At pH 8, the amplitude of the slowest rate constant gradually increases over the first 3 hours and a half, whereas at pH 9.4 the amplitude decreases until no effect is detected.

## 4 Discussion

The interaction of tetryl and BRC yields two observable effects. First, the rate of formation of a coloured product between tetryl and detergent is amplified by the presence of BRC, and second, the charge recombination of  $P^+Q^-$  proceeds slower in the presence of tetryl. The kinetics and optical spectra collected give information on the nature of the product and possible reaction, evidence on the binding of tetryl to BRC and on the location of the binding and reactions and provide insight as to possible mechanisms of the interaction, linking both effects together.

### 4.1 Reaction of tetryl with nucleophile-containing detergents

Because of the strong electron withdrawing nitro groups positioned around the ring, the head methyl nitramine group of tetryl is a good site for nucleophilic substitution. From the resonance structures shown below (Figure 29), the stability of the carbocation at the head group site of tetryl originates from the electronegative nitrogen bound to the ring, and from the higher stability of tertiary carbocations over secondary carbocations. These resonance structures show that there is a lower electron density at the carbon in the ring attached to the head group of the explosive, making it the best site for an electronegative atom or group to attack.

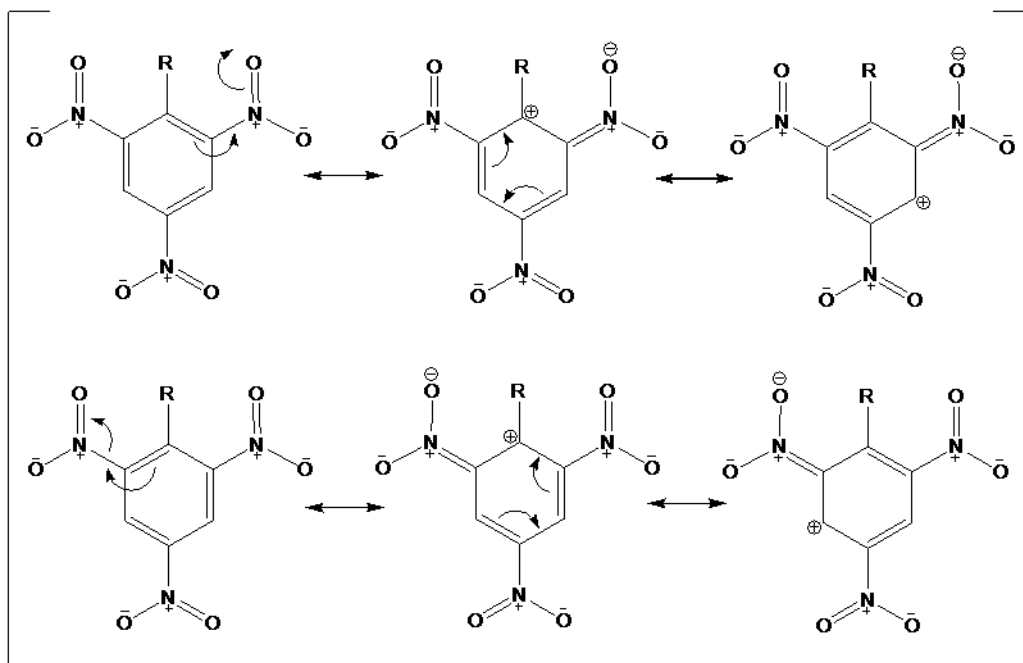


Figure 29: Some resonance structures for all trinitrobenzene derived explosives.

In the case of tetryl hydrolysis, the electronegative oxygen atom from a water molecule or hydroxyl group can attack the site and replace the methylnitramine group with an OH group. This reaction forms a Meisenheimer complex, where both the leaving group and hydroxyl group stay attached to the ring to form a relatively stable intermediate.<sup>32</sup> It is possible other nucleophilic oxygen-containing molecules can undergo a similar mechanism of reaction.

#### 4.1.1 Probing the environment: Absorbance spectra of picric acid

The absorbance spectrum of picric acid is sensitive to its environment, as shown in Figure 20. As LDAO concentration is increased, the peaks are shifted in opposite directions. The shift in the spectrum reflects an increase in the energy of the absorbance in the case of the blueshift and a decrease in the case of the redshift. These are caused by changes in the polarizability of the electron. The presence of LDAO decreases the dielectric constant of the environment, as it increases the hydrophobicity of the solvent. A change in dielectric environment will affect the energy of the dipoles experienced by the electron.<sup>28</sup>

The same is seen with the tetryl and detergent reaction product. At a concentration of 5% LDAO, the product peak at 415 nm is shifted similarly by about 5 nm to the red (Figure 19). Like with picric acid, the peak positions of the reaction product can be used to probe the dielectric properties of the environment.

#### 4.1.2 Product identification: Absorbance spectra of reaction products

We suggest the electronegative oxygen of either detergent can act as a strong enough nucleophile to replace the head group of tetryl (Figure 30), similar to the attack by the oxygen in water in the case of hydrolysis. The nitrogen in the methylamine is also electronegative, making it a good leaving group. It is less electronegative than oxygen, which allows for the substitution to take place.

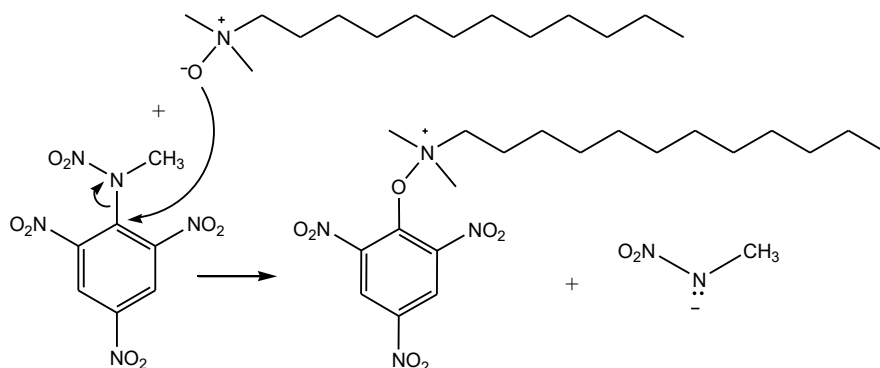


**Figure 30: Possible reaction mechanism and product between tetryl and LDAO.**

As seen in Figure 19A, the spectrum of the product of tetryl in the presence of LDAO and BRC or detergent alone is not picric acid. The spectra are similar, but the peaks are not at the same positions, suggesting a

similar product is formed. The spectra of the tetryl product with or without protein are the same, suggesting that the presence of protein does not yield a new product, but amplifies the reaction that occurs in the buffer.

When TX-100 is used as the detergent (Figure 19B), a similar observation is made. The tetryl product spectra do not match the spectrum of picric acid with triton. A new product, different from the one created with LDAO is formed. In the presence of protein, the spectrum of the product with 0.1% triton matches the spectrum of the product without protein in 5% triton. This could be caused by the product being in a different environment, with higher local detergent concentration.

#### 4.1.3 Reagent determination: reaction kinetics with LDAO

The observed reaction rate constant is dependent on the concentration of LDAO (Figure 24). When 100  $\mu\text{M}$  tetryl is used, the rate constants found from the biexponential fits were linearly dependent on the concentration of LDAO, indicative of a second order collisional reaction. LDAO is a reagent for the formation of the visible product with peaks at 345 nm and 415 nm.

The reaction kinetics are biexponential, showing that there must be two different environments for the reaction. The presence of detergent past its critical micellar concentration, or CMC, the concentration at which the detergents begin to form micelles in solution, causes the system to be biphasic. There is the higher dielectric environment of the aqueous phase, and the lower dielectric environment of the interior of the micelles. It is possible there are different rates for inside and outside micelles. First, the tetryl molecules are not equally partitioned in both phases. They have poor water solubility, so they are likely mostly dispersed by the micelles. Still, a proportion of tetryl will remain in the aqueous phase. Additionally, like tetryl, the concentration of LDAO is not equally partitioned, as there are molecules packed into micelles, and others that are less locally concentrated in bulk solvent. The heterogeneity of the solution in terms of reagent concentrations could be what is giving rise to different rate constants. Likely, the micelles would be the location of the higher rate constant, since both tetryl and LDAO are present in higher concentration in this environment. However, much more empty micelles are needed to get a similar rate to micelles containing BRC. At 0.1 % LDAO concentration, about 4 mM, there is a rate constant of around  $2 \times 10^{-2} \text{ min}^{-1}$  (Figure 24). The slower rate associated with the presence of protein of  $1.6 \times 10^{-2} \text{ min}^{-1}$  is present with only 1  $\mu\text{M}$  BRC present in micelles (Figure 21). At around 75-100 LDAO molecules per micelle,<sup>33,34</sup> there is as much as 1  $\mu\text{M}$  LDAO micelles containing BRC, corresponding to 100  $\mu\text{M}$  of LDAO contained in micelles, if only one BRC molecule is present inside a micelle. In the presence of

BRC, an order of magnitude less micellar LDAO is required than in the absence of protein to obtain a similar rate. There is still a notable difference caused by the presence of BRC on the reaction kinetics.

The amplitude of the faster component also increases as LDAO concentration is increased, while the slow component decreases. As LDAO concentration is increased past the CMC, more micelles are formed, which increases the ratio of micellar LDAO to bulk LDAO. This would increase the amplitude of the component due to tetryl reacting with micellar LDAO versus bulk LDAO. This is also shown by the shift in absorbance of the spectrum of the product at higher LDAO concentration (Figure 19A).

The pH affects the reaction without protein (Figure 23). The rate is approximately 10-fold slower with 0.025% LDAO and 100  $\mu\text{M}$  tetryl at pH 8 than at pH 9.4. It is possible the reaction is base-catalysed, where OH is needed to make an initial attack on the tetryl. The lower pH could also stabilize the leaving methyl nitramine group of the tetryl.

The reaction kinetics follow the same model regardless of pH. Even when the reaction occurs more slowly at pH 8, there is still the detection of two reaction sites in R26 strain, and one in WT that is faster than the rate in buffer alone. There is likely no protonation or deprotonation of the protein at this range that affects the interaction of tetryl with the protein at the two sites.

#### 4.2 Evidence of tetryl binding to BRC – concentration dependence

From Figure 25, there is an apparent tetryl concentration dependence on the amplitude of tetryl reacting with the fast kinetics over the range of 10  $\mu\text{M}$  to 100  $\mu\text{M}$  tetryl. At higher concentrations than 100  $\mu\text{M}$ , the product formation from tetryl takes longer than a day to complete, whereas the protein degrades in solution when kept at these conditions at room temperature over several hours. The protein-dependent kinetics obtained from a run using higher tetryl concentration (around 500  $\mu\text{M}$ ) would not be representative of kinetics using entirely native protein. Additionally, at 500  $\mu\text{M}$  tetryl, there is some precipitate. The kinetics for the reaction with higher tetryl concentration than 100  $\mu\text{M}$  could not be obtained.

Nonetheless, the concentration dependence seen over this short interval suggests binding between tetryl and LDAO associated to the protein. Each exponential component of the fits must represent a different site for the reaction. The site responsible for the fastest rate constant (around  $5 \times 10^{-2} \text{ min}^{-1}$  in R26) remains unoccupied when only 10  $\mu\text{M}$  tetryl is used. When more tetryl is used, there is a higher ratio of the tetryl reacting with the fastest rate constant. This suggests the presence of first order binding kinetics, although not enough data could be obtained to obtain a  $K_D$ .

The dependence of the BRC charge recombination on the concentration of tetryl reveals a binding interaction between tetryl and BRC (Figure 26). As more tetryl is added, there is an increase in amplitude of the long-lived charge separated state, with a recombination rate constant of  $0.01 \text{ s}^{-1}$ , while the rate constants remain relatively constant. This is indicative of first order binding, since the observed rate constants are independent of the tetryl concentration. The long-lived charge separated state represents a conformation of the protein bound to tetryl.

Additionally, the changes in the spectrum of the BRC cofactors indicate precise and stable changes in the environment of the cofactors. From the fittings shown in Figure 17, the difference spectrum shows changes in the dimer and one of the two monomers. The bleaching, shifts and band broadening that could be used to interpret this spectrum would be due to changes in the energetics of the absorbing electrons, which could be due to changes in the dielectric environment or in the introduction of a charge or dipole near the absorbing electrons. These changes seen in the R26 strain are introduced by the presence of tetryl, suggesting this molecule has a precise and fixed location inside the cavity, where it will interact with the cofactors or change the environment of the cavity.

### 4.3 Location of interactions

Evidence is shown as to the location of both observed interactions. By observing the presence of different kinetic parameters of the evolution of the tetryl reaction product in different conditions, different locations could be inferred. Also, the changes in the BRC spectrum in the presence of tetryl show where the binding takes place.

#### 4.3.1 Tetryl-detergent reaction

The presence of BRC amplifies the reaction between tetryl and LDAO. The reaction occurs at 3 notable locations. In the absence of protein, tetryl reacts with LDAO molecules that make up the micelles, with an observed rate constant of  $2.0 \times 10^{-4} \text{ min}^{-1}$  when 0.025% LDAO is present in the buffer (Figure 21). This slow rate constant is also observable in 0.1% TX-100 detergent, and with either detergent in the presence of WT strain BRC. This rate constant is associated to the rate of tetryl reacting with bulk detergent, not associated to the protein.

The second and third components, with rate constants around  $1.6 \times 10^{-2} \text{ min}^{-1}$  and  $7.7 \times 10^{-2} \text{ min}^{-1}$ , are only observed in the presence of protein for 0.025% LDAO concentrations. The fastest rate constant is only observable in the presence of R26 strain BRC, with LDAO detergent. When LDAO is present, it will occupy the empty carotenoid binding site of the carotenoid-less R26 strain BRC (Figure 31). A tetryl molecule likely reacts with the LDAO present at this site. In WT (Figure 21), the carotenoid blocks the

LDAO from binding and tetryl from entering. Triton enters the cavity but does not occupy the carotenoid site due to size and energetic restrictions. If TX-100 is used with R26 strain (Figure 21), there is no LDAO in the cavity present for this rate to occur. Last, the R26 protein in the presence of LDAO also loses this rate when illuminated (Figure 22A). The LDAO in the carotenoid site is close to the dimer (Figure 31B), which is positively charged in the light. The positive charge on the dimer must either provide an unfavourable environment for the binding of tetryl or inhibit the reaction from occurring.

The slower of the two protein-amplified reactions is likely a more general site. All situations with protein show one kinetic component with a rate constant of around  $2 \times 10^{-2} \text{ min}^{-1}$ . Wild-type and R26 strains both show this reaction, so the location cannot be in the carotenoid binding site (Figure 21). When R26 or WT is illuminated, the slower protein-amplified reaction still occurs (Figure 22). This means the charges inside the cavity on the Q and the P do not affect this specific reaction location, whereas the carotenoid site reaction is completely inhibited. The slow reaction cannot take place near the dimer or the quinone, which occupy a large part of the cavity (Figure 31). Last, in the presence of TX-100, which cannot enter the carotenoid binding site, the slow protein-amplified reaction is present (Figure 21B). The product spectrum in the presence of protein with 0.1% TX-100 matches the spectrum of tetryl and 5% TX-100 without protein (Figure 19). It is likely the product in the presence of protein remains bound to an environment with high local Triton concentration. The protein-micelle interface would provide such an environment with high local Triton concentration. It also has a lower dielectric constant than the bulk, which would more easily accommodate the hydrophobic tetryl and even more hydrophobic tetryl-TX-100 product.

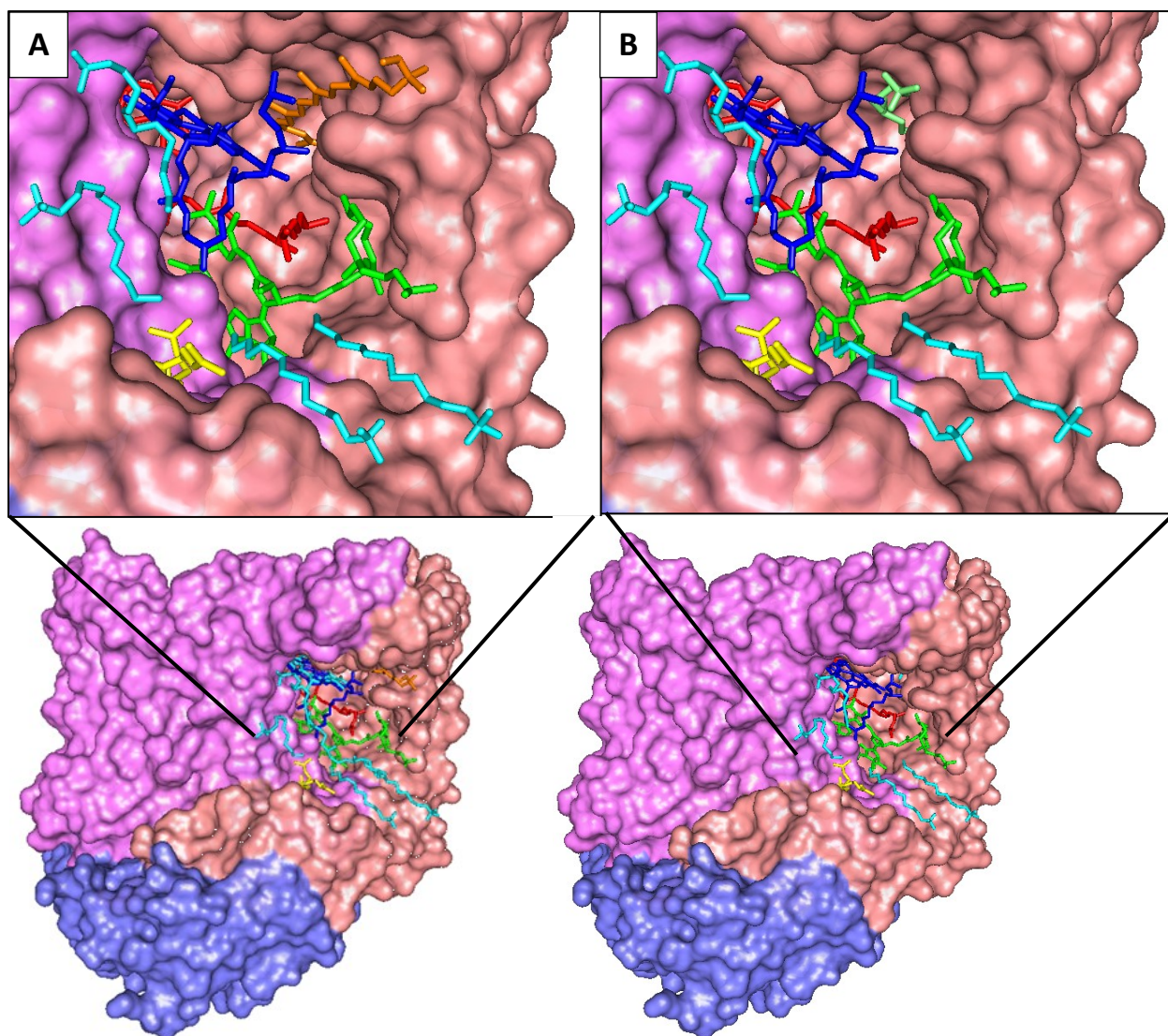


**Figure 31: Pymol structure of BRC cavity with cofactors: dimer (red), monomer (blue), bacteriopheophytin (green) and ubiquinone (yellow). (A) WT-strain BRC, with carotenoid (orange) present in binding site, PDB code 2UXK.<sup>35</sup> (B) R26-strain BRC, with LDAO (lime) present in the carotenoid binding site, PDB 1RG5.<sup>36</sup> LDAO molecules present in the cavity but not in the carotenoid binding site are coloured in light blue.**

#### 4.3.2 Charge recombination

Previously, it has been found that conformational changes of mutant BRC, where amino acids near the dimer have been changed to remove residues hydrogen bonding to the dimer, can block conformational changes causing long-lived charge separated states with slower charge recombination rates. This has been attributed to light-induced conformational changes occurring near the dimer, whereas previous attention

had been on conformational changes occurring in the light near the quinone, which only cause a charge recombination rate of  $0.1 \text{ s}^{-1}$ . These processes were explained to be occurring consecutively, where the changes near the dimer only happen after the changes near the quinone, as shown in Figure 9.<sup>13,14</sup>

The increasing concentration of tetryl has a similar effect on the kinetics (Figure 25). The increase in amount of the C3 conformer (with a charge recombination rate of  $0.01 \text{ s}^{-1}$ ) appears to happen consecutively to the increase in the intermediate rate of  $0.1 \text{ s}^{-1}$ , associated to light-induced conformational changes around the quinone (C2 conformer). The tetryl likely binds near the dimer and inactive bacteriochlorophyll monomer ( $B_b$ ), where it changes the energetics of the oxidized dimer by forming favourable intermolecular interactions with it to stabilize it, decreasing the charge recombination rate to  $0.01 \text{ s}^{-1}$ . The vicinity of this monomer was the site where conformational changes were previously found to occur. The deprotonation of M210 tyrosine, rotation of the 2-acetyl group of the monomer B and proton release have been reported to cause the conformational change with a charge recombination rate of  $0.01 \text{ s}^{-1}$ .<sup>13-15</sup>

Additionally, the changes in the R26 BRC difference spectrum are consistent with the presence of tetryl in the cavity near the carotenoid binding site, affecting the absorbance spectra of the dimer and one of the monomers (Figure 17). The changes in the spectra of the BRC cofactors can be best fit to either of two following models. In the first one (Figure 17A), the dimer loses absorbance, and the monomer  $B_b$ , the monomer in the cavity with the carotenoid, is blue shifted. This supports the idea that tetryl is found near the carotenoid site in the cavity. There, it can make energetically unfavourable interactions with the monomer B and shift the absorbance of monomer B to higher energy. The decrease in absorbance in the dimer could be due to the decrease in the oscillator strength of the dimer, which would decrease the extinction coefficient.

The second model involves changes near the monomer A, which is in the other side of the cavity, further away from the carotenoid. Still, in this model, it is possible that the tetryl introduction causes conformational changes around the whole cavity that would broaden both monomer peaks, but its proximity to the monomer B prevents the changes to this monomer. The changes also would cause a redshift to the dimer, which would be caused by a stabilizing favourable interaction between the tetryl and the dimer, and, as in the previous model, a decrease in the oscillator strength of the dimer, lowering the absorbance. However, the first model appears to best explain the spectral changes with fewer changes, so it seems more likely.

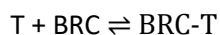
#### 4.4 Proposed mechanism

The presence of tetryl increases the lifetime of the charge separated state by binding to the protein with a  $K_D$  of 60  $\mu\text{M}$  and increasing the relative amount of protein that are in a long-lived charge separated state (Figure 26) recovering with a rate constant of  $0.01 \text{ s}^{-1}$ , 100-fold slower than in dark-adapted protein.

We propose two possible mechanisms to explain this. Either the tetryl itself is responsible for stabilizing the charged dimer, or it is the reaction product with LDAO that accomplishes this. In the first model, illustrated by Figure 32, the stabilization of the dimer by tetryl and the reaction of tetryl with LDAO are competing processes. In this case, the presence of tetryl would cause the stabilization of the dimer and the presence of the component with a slower charge recombination rate. The product would have no effect on the charge recombination kinetics. The binding site is similar or the same for both the reaction and the charge-separation stabilization: near the dimer, at the carotenoid site.

Competitive reactions would explain why the effect of tetryl on the charge recombination of the protein is higher at pH 8 (Figure 27), where tetryl reacts slower with LDAO than at pH 9.4 (Figure 23). If more tetryl is left unchanged, it can remain near the dimer where it will stabilize the charge and cause the recombination to occur with a rate constant of  $0.01 \text{ s}^{-1}$ .

At pH 8, there is an initial increase in the relative amount of long-lived charge-separated protein over tetryl incubation time (Figure 27). It is possible that tetryl requires time to fill the cavity. The tetryl must first reach the cavity, which it must do rapidly, since the reaction appears to occur instantly. The tetryl must then be present in large enough concentration in the cavity for the protein to undergo charge recombination with a rate constant of  $0.01 \text{ s}^{-1}$ . The time delay seen for the emergence of the tetryl-bound conformation in Figure 27 could be caused by the time it takes for tetryl to fill the cavity. After 3 hours and a half, nearly half of the tetryl has reacted. If the reaction product does not stabilize the dimer, but instead diffuses out of the cavity, then the effect of tetryl on the charge recombination will begin to decrease. The process can be described by the following association/dissociation equilibrium equation



where T is unbound tetryl, BRC is unbound protein, and BRC-T is when tetryl is associated to the protein, causing a conformation change to the C3 conformer. As less tetryl remains inside the cavity, there is a shift in equilibrium towards the left-hand-side of the equation, the unbound state, by Le Châtelier's principle.

At pH 9.4, there is the same initial effect of tetryl on the charge recombination kinetics as for pH 8. Initially, the same amount of tetryl will enter the cavity, as the pH did not change the amount of tetryl interacting with the protein. Only the rate of the product-forming reaction is slower at lower pH (Figure 23). Since the tetryl reacts faster at pH 9.4, the effect decreases over time as the available tetryl in the cavity is rapidly depleting.

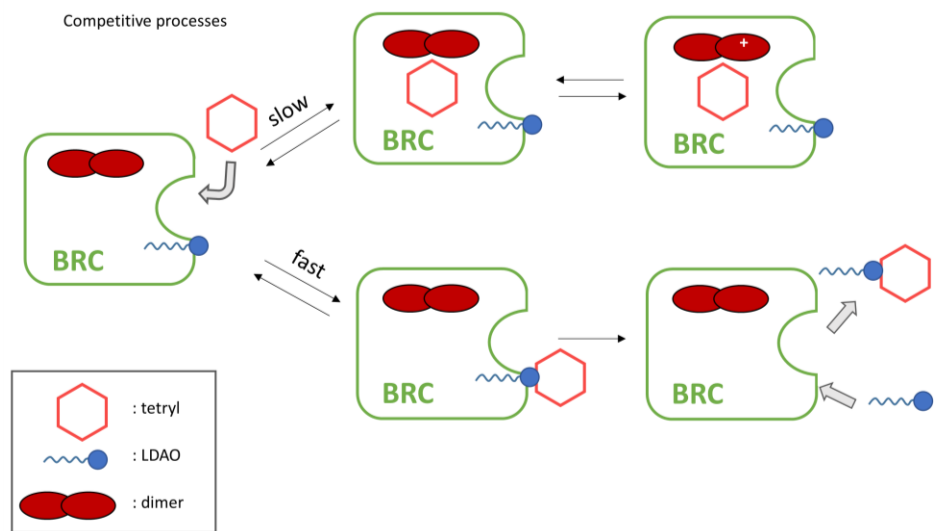


**Figure 32: Schematic of proposed competitive processes for the BRC-amplified tetryl-LDAO reaction and the stabilization of the charge separated state of BRC. The reaction of tetryl with the LDAO in the carotenoid site occurs at a fast rate (lower branch), whereas the occupation of the cavity by tetryl occurs more slowly (upper branch). In this model, tetryl must occupy the cavity in order to stabilize the charge separated state.**

In the second model, illustrated in Figure 33, the reaction product of tetryl and LDAO stabilizes the charge separated state. This implies the reaction of tetryl and LDAO and the stabilization of the dimer are successive processes. Tetryl binds to the LDAO molecule in the carotenoid site near the dimer, where it reacts with LDAO. At first, the high local concentration of tetryl and LDAO drives the replacement of the tetryl-LDAO product with LDAO and tetryl in the binding site. As more tetryl-LDAO product is formed, the binding site can be more and more occupied with the product because of its increased concentration, even if its affinity were lower than the reagent's. The tetryl-LDAO product bound to the protein accumulates over time. The bound state stabilizes the dimer, slowing the charge recombination of the protein upon illumination. After an initial increase over time of product-bound protein with a corresponding charge recombination rate constant of  $10^{-2} \text{ s}^{-1}$ , the tetryl-LDAO product diffuses out of the

protein. When no more tetryl remains to continue reacting and binding to the carotenoid site, only the diffusion out of the protein causes the amount of product-bound protein to decrease, and the amount of protein with a  $10^{-2} \text{ s}^{-1}$  rate constant decreases.

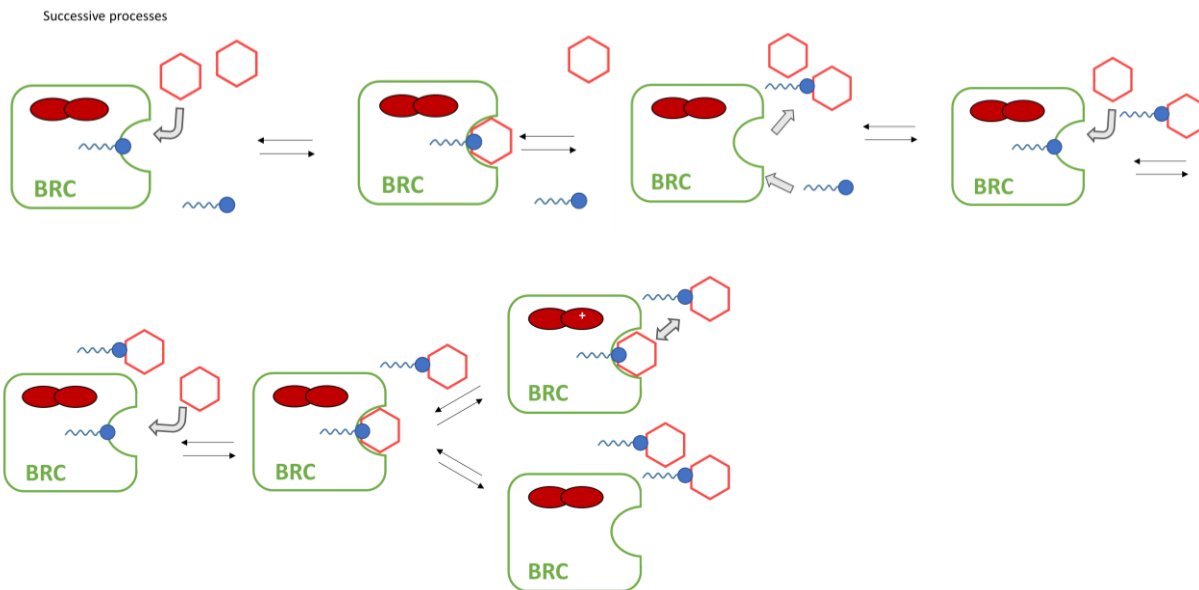


**Figure 33: Schematic of proposed successive processes for the BRC-amplified tetryl-LDAO reaction and the stabilization of the charge separated state of BRC. In this model, the tetryl-LDAO product is responsible for stabilizing the charge-separated state of the protein. The tetryl must first react to form enough product to drive the equilibrium towards the occupation of the binding site in the cavity by product.**

#### 4.5 Effect of interaction – biosensing signal amplification and charge-storage capacity

As previously stated in the objective, the ultimate goal of the study of these interactions is to harness them for biosensing as well as for the creation of solar-powered charge storage devices. For the biosensor, both the formation of product and the change in charge recombination kinetics can be used to create a bimodal sensor, using optics and electrochemistry. The effect of tetryl on charge recombination kinetics can be used as an excessively simple starting point to create a device that can store charges over a longer time using sunlight, which can be paired to energetically unfavourable processes requiring charges.

##### 4.5.1 Biosensing

In the presence of R26 BRC, the overall reaction of tetryl and LDAO is observed to occur 30-fold faster than in the absence of BRC (Figure 21). This means that at this concentration, the presence of protein could help detect the explosive 30 times faster or could amplify the signal 30 times the signal generated

without protein, depending on the needs of the detection. Additionally, it was shown that at 500 nM, the product is still detectable, with a signal-to-noise ratio of around 5 (Figure 25). This shows a preliminary limit of detection in the nanomolar range, which corresponds to around 140 ppb. Many other biosensors, often requiring more complex designs or methods of detection, fall in the ppb range for LODs.<sup>16</sup>

The presence of tetryl also affects the charge recombination kinetics of the protein. When 50  $\mu\text{M}$  tetryl are present with 1  $\mu\text{M}$  R26 BRC, there is 30% of the charge-separated protein population recovering with the rate constant of  $0.01\text{ s}^{-1}$  (Figure 26), corresponding to conformation changes near the dimer. Even in the presence of 5  $\mu\text{M}$  tetryl, the charge recombination kinetics are visibly altered. To utilise these observed changes in electron transfer rates, the protein would need to be immobilized on a conducting surface that would act as an electrode. Upon illumination, the electron transfer would generate a current that can reach the electrode. If secondary electron donors are present in the electrochemical cell, they can re-reduce the positively charged dimer so that the current can continue in the light. In the presence of tetryl, the positive charge on the dimer is stabilized. With a secondary donor with a finely tuned redox potential, the oxidized dimer may accept less electrons in this case. This could potentially be observed as a reduction of photocurrent over time in the light in the presence of tetryl.

There are several advantages to utilizing this machinery for biosensing. The protein is found naturally in bacteria that are very easy and relatively inexpensive to grow, as compared to PSII found in plants. The protein could be immobilized on an indium-tin-oxide (ITO) surface, by simply functionalizing the surface first with cytochrome c, as has been previously reported.<sup>37</sup> This would assure the orientation of the protein would be uniform, maximizing the summative effect of the current. Another method would be to use nickel-nitrilotriacetic acid (Ni-NTA)/His tag system, where a tag containing several His residues is added to the protein. This tag has no effect on the overall structure and function of the BRC. The uncharged nitrogen atoms in the His rings bind strongly to  $\text{Ni}^{2+}$ , forming a ligand. The ITO surface can be functionalized with Ni-NTA, while the His tag was found to be added preferentially to the dimer side of the BRC, giving the BRC a preferential direction when bound to the surface.<sup>38</sup>

Using ITO for the surface of a biosensor has many advantages. It is first very inexpensive. Second, it is transparent, making it ideal for optical sensing as well. It can also conduct current, so it has both attributes necessary for its use in a bimodal optical/electrochemical biosensor.<sup>39</sup>

The bimodality of this system, and the selectivity of the protein for tetryl improves the specificity of the detection for tetryl, when an exact identification of contaminant or of hazardous materials is necessary. The product also absorbs at a longer wavelength than tetryl, making it easier for optical detection. Tetryl

has absorbance in shorter UV wavelength range, around 200 nm. The product appears visibly yellow and can be detected using the 415-nm peak, which is in the visible range. UV light sources are more expensive than visible light and present some health concerns. Additionally, many clear materials have absorption in the UV range. Much less consideration would need to be made for the selection of transparent materials for optical detection.

#### 4.5.2 Charge storage device

The relative ease to grow bacteria that produce the BRC also makes it an ideal starting material for the creation of charge storage devices. The use of biological material is a strategy based on the idea that these proteins are already very optimized over millions of years of evolution to generate a charge separation with sunlight, a renewable source that produces no harmful waste when harnessed for photosynthesis. The binding of tetryl to the protein can convert up to at least 70 % of the protein to the tetryl-bound long-lived conformation, which has a charge recombination rate constant of  $0.01 \text{ s}^{-1}$ , 100 times slower than in the case of the dark-adapted protein.

Concretely, the tetryl-bound protein conformation could be generated to donate electrons or to give energy to a process that requires a charge or energy, much like how a battery or capacitor is used to provide a current. The presence of tetryl allows the protein to be paired to processes occurring up to 100 times slower than if the protein were alone, as the kinetics of the paired process need to be at least as fast as the charge recombination kinetics of the protein, or the protein could not transfer electrons or energy in any form. The charge recombination would thus be in a competing process to the paired reaction.

Previously, to obtain these long-lived conformations, the creation of mutants or the incorporation of the protein into liposomes were necessary.<sup>13-15</sup> Both these methods are much more complicated than a simple tetryl binding process. The former requires the use of molecular biology tools to guide point mutations to important amino acids. The latter requires a lengthy protocol for liposomal incorporation, that can leave much of the proteins damaged or unincorporated, producing low yields. However, these methods previously developed in our lab yielded kinetics 10 times slower than in the presence of tetryl. The best method is thus dependent on the requirements of the specific process.

## 5 Conclusion

The interaction between tetryl and BRC causes two observable effects: the amplification of the reaction between tetryl and LDAO, and the increase in time of the  $P^+Q^-$  charge recombination. The protein provides two favourable locations for the reaction to occur: in the cavity containing several LDAO molecules, where the reaction occurs 80-fold faster than in bulk buffer with detergent, and in the carotenoid binding site when the carotenoid is absent, where it reacts 400-fold faster than in bulk.

Tetryl or its reaction product also appears to bind near the dimer and monomer B to stabilize the charge on the dimer. This increases the amount of protein with charges recovering at a rate 100-fold slower than when protein is in the dark-adapted conformation.

For detection purposes, both effects could be combined in a bimodal biosensor. The change in absorbance at 345 nm could be monitored to detect tetryl concentrations in solution as low as 500 nM. Also, the change in charge recombination kinetics can be detected as a change in light-induced current across a monolayer of protein. A biosensor could be constructed by self-assembled monolayers of cytochrome c and BRC on ITO surfaces, which is transparent and conducting to allow for both optical and electrochemical modes of detection.

Last, the use of tetryl-bound BRC offers a very simple preparation method and use for the starting design of a bio-hybrid charge storage device. The addition of tetryl allows for the BRC charge separation to be paired to energy-inefficient processes up to 100-fold slower than for unchanged native BRC. The effects of this reaction can also inspire the design of purely artificial photosynthetic devices with longer charge-separated lifetimes.

## 6 References

1. Okamura, M. Y., Paddock, M. L., Graige, M. S. & Feher, G. Proton and electron transfer in bacterial reaction centers. *Biochim. Biophys. Acta BBA - Bioenerg.* **1458**, 148–163 (2000).
2. Blankenship, R. E. Origin and early evolution of photosynthesis. *Photosynth. Res.* **33**, 91–111 (1992).
3. Ort, D. R. & Yocum, C. F. *Oxygenic Photosynthesis: The Light Reactions*. (Springer Science & Business Media, 2006).
4. Emerson, R. & Arnold, W. The Photochemical Reaction in Photosynthesis. *J. Gen. Physiol.* **16**, 191–205 (1932).
5. Heathcote, P., Jones, M. R. & Fyfe, P. K. Type I photosynthetic reaction centres: structure and function. *Philos. Trans. R. Soc. Lond. B Biol. Sci.* **358**, 231–243 (2003).
6. Loll, B., Kern, J., Saenger, W., Zouni, A. & Biesiadka, J. Towards complete cofactor arrangement in the 3.0 Å resolution structure of photosystem II. *Nature* **438**, 1040 (2005).
7. Fujii, R. *et al.* Structure of the carotenoid bound to the reaction centre from *Rhodobacter sphaeroides* 2.4.1 revealed by time-resolved X-ray crystallography. *Protein Database* (2009).
8. Feher, G., Allen, J. P., Okamura, M. Y. & Rees, D. C. Structure and function of bacterial photosynthetic reaction centres. *Nature* **339**, 111–116 (1989).
9. Marcus, R. A. On the theory of oxidation-reduction reactions involving electron transfer. I. *J. Chem. Phys.* **24**, 966–978 (1956).
10. Kleinfeld, D., Okamura, M. Y. & Feher, G. Electron transfer in reaction centers of *Rhodospseudomonas sphaeroides*. I. Determination of the charge recombination pathway of D<sup>+</sup> QAQ<sup>-</sup> B and free energy and kinetic relations between Q<sup>-</sup> AQB and QAQ<sup>-</sup> B. *Biochim. Biophys. Acta BBA-Bioenerg.* **766**, 126–140 (1984).
11. Gopher, A. *et al.* The effect of an applied electric field on the charge recombination kinetics in reaction centers reconstituted in planar lipid bilayers. *Biophys. J.* **48**, 311 (1985).

12. Stowell, M. H. *et al.* Light-induced structural changes in photosynthetic reaction center: implications for mechanism of electron-proton transfer. *Science* **276**, 812–816 (1997).
13. Deshmukh, S. S., Williams, J. C., Allen, J. P. & Kálmán, L. Light-Induced Conformational Changes in Photosynthetic Reaction Centers: Dielectric Relaxation in the Vicinity of the Dimer. *Biochemistry* **50**, 340–348 (2011).
14. Deshmukh, S. S., Williams, J. C., Allen, J. P. & Kálmán, L. Light-Induced Conformational Changes in Photosynthetic Reaction Centers: Redox-Regulated Proton Pathway near the Dimer. *Biochemistry* **50**, 3321–3331 (2011).
15. Deshmukh, S. S., Akhavein, H., Williams, J. C., Allen, J. P. & Kalman, L. Light-induced conformational changes in photosynthetic reaction centers: impact of detergents and lipids on the electronic structure of the primary electron donor. *Biochemistry* **50**, 5249–5262 (2011).
16. Singh, S. Sensors—An effective approach for the detection of explosives. *J. Hazard. Mater.* **144**, 15–28 (2007).
17. Ju, K.-S. & Parales, R. E. Nitroaromatic compounds, from synthesis to biodegradation. *Microbiol. Mol. Biol. Rev.* **74**, 250–272 (2010).
18. Brill, T. B. & James, K. J. Kinetics and mechanisms of thermal decomposition of nitroaromatic explosives. *Chem. Rev.* **93**, 2667–2692 (1993).
19. Rensen, J. van, Van der Vet, W. & Vliet, W. van. Inhibition and uncoupling of electron transport in isolated chloroplasts by the herbicide 4, 6-dinitro-o-cresol. *Photochem. Photobiol.* **25**, 579–583 (1977).
20. Thévenot, D. R., Toth, K., Durst, R. A. & Wilson, G. S. Electrochemical biosensors: recommended definitions and classification. *Anal. Lett.* **34**, 635–659 (2001).

21. Carpentier, R., Lemieux, S., Mimeault, M., Purcell, M. & Goetze, D. C. A photoelectrochemical cell using immobilized photosynthetic membranes. *J. Electroanal. Chem. Interfacial Electrochem.* **276**, 391–401 (1989).
22. Bhalla, V., Zhao, X. & Zazubovich, V. Detection of explosive compounds using Photosystem II-based biosensor. *J. Electroanal. Chem.* **657**, 84–90 (2011).
23. Bhalla, V. & Zazubovich, V. Self-assembly and sensor response of photosynthetic reaction centers on screen-printed electrodes. *Anal. Chim. Acta* **707**, 184–190 (2011).
24. Panda, M. K., Ladomenou, K. & Coutsolelos, A. G. Porphyrins in bio-inspired transformations: Light-harvesting to solar cell. *Coord. Chem. Rev.* **256**, 2601–2627 (2012).
25. Bhalla, V. & Zazubovich, V. Immobilization and nanoscale film structure of bacterial reaction centers on gold. *Surf. Sci.* **606**, 1323–1326 (2012).
26. Van Holde, K. E., Johnson, W. C. & Ho, P. S. Chapter 8: Quantum Mechanics and Spectroscopy. in *Principles of physical biochemistry* (Upper Saddle River, 2006).
27. Zhu, J., van Stokkum, I. H. M., Paparelli, L., Jones, M. R. & Groot, M. L. Early Bacteriopheophytin Reduction in Charge Separation in Reaction Centers of *Rhodobacter sphaeroides*. *Biophys. J.* **104**, 2493–2502 (2013).
28. Grdadolnik, J. Infrared difference spectroscopy: Part I. Interpretation of the difference spectrum. *Vib. Spectrosc.* **31**, 279–288 (2003).
29. James Frederick Hurley. Section 8.3: First order linear differential equations. in *Intermediate Calculus: Multivariable Functions and Differential Equations with Applications* 513–524 (Saunders College, 1980).
30. Peter Atkins & Julio de Paula. Section 22.7: Consecutive elementary reactions. in *Physical Chemistry* 811–819 (W. H. Freeman and Co., 2006).

31. Kayser, E. G., Burlinson, N. E. & Rosenblatt, D. H. *Kinetics of Hydrolysis and Products of Hydrolysis and Photolysis of Tetryl*. (NAVAL SURFACE WEAPONS CENTER SILVER SPRING MD, NAVAL SURFACE WEAPONS CENTER SILVER SPRING MD, 1984).
32. Hubert, C., Dossmann, H., Machuron-Mandard, X. & Tabet, J.-C. ESI formation of a Meisenheimer complex from tetryl and its unusual dissociation. *J. Mass Spectrom.* **48**, 306–311 (2013).
33. Herrmann, K. W. Non-Ionic—Cationic Micellar Properties of Dimethyldodecylamine Oxide. *J. Phys. Chem.* **66**, 295–300 (1962).
34. Strop, P. & Brunger, A. T. Refractive index-based determination of detergent concentration and its application to the study of membrane proteins. *Protein Sci.* **14**, 2207–2211 (2005).
35. Koepke, J. *et al.* pH modulates the quinone position in the photosynthetic reaction center from *Rhodobacter sphaeroides* in the neutral and charge separated states. *J. Mol. Biol.* **371**, 396–409 (2007).
36. Roszak, A. W. *et al.* Protein regulation of carotenoid binding: gatekeeper and locking amino acid residues in reaction centers of *Rhodobacter sphaeroides*. *Structure* **12**, 765–773 (2004).
37. El Kasmi, A. *et al.* Adsorptive immobilization of cytochrome c on indium/tin oxide (ITO): electrochemical evidence for electron transfer-induced conformational changes. *Electrochem. Commun.* **4**, 177–181 (2002).
38. Trammell, S. A., Spano, A., Price, R. & Lebedev, N. Effect of protein orientation on electron transfer between photosynthetic reaction centers and carbon electrodes. *Biosens. Bioelectron.* **21**, 1023–1028 (2006).
39. Kim, H. *et al.* Electrical, optical, and structural properties of indium–tin–oxide thin films for organic light-emitting devices. *J. Appl. Phys.* **86**, 6451–6461 (1999).